6 Gravity surveying

6.1 Introduction

In gravity surveying, subsurface geology is investigated on the basis of variations in the Earth's gravitational field arising from differences of density between subsurface rocks. An underlying concept is the idea of a *causative body*, which is a rock unit of different density from its surroundings. A causative body represents a subsurface zone of anomalous mass and causes a localized perturbation in the gravitational field known as a gravity anomaly. A very wide range of geological situations give rise to zones of anomalous mass that produce significant gravity anomalies. On a small scale, buried relief on a bedrock surface, such as a buried valley, can give rise to measurable anomalies. On a larger scale, small negative anomalies are associated with salt domes, as discussed in Chapter 1. On a larger scale still, major gravity anomalies are generated by granite plutons or sedimentary basins. Interpretation of gravity anomalies allows an assessment to be made of the probable depth and shape of the causative body.

The ability to carry out gravity surveys in marine areas or, to a lesser extent, from the air extends the scope of the method so that the technique may be employed in most areas of the world.

6.2 Basic theory

The basis of the gravity survey method is Newton's Law of Gravitation, which states that the force of attraction F between two masses m_1 and m_2, whose dimensions are small with respect to the distance r between them, is given by

$$F = \frac{Gm_1m_2}{r^2} \tag{6.1}$$

where G is the Gravitational Constant (6.67×10^{-11} $m^3\,kg^{-1}\,s^{-2}$).

Consider the gravitational attraction of a spherical, non-rotating, homogeneous Earth of mass M and radius R on a small mass m on its surface. It is relatively simple to show that the mass of a sphere acts as though it were concentrated at the centre of the sphere and by substitution in equation (6.1)

$$F = \frac{GM}{R^2}m = mg \tag{6.2}$$

Force is related to mass by an acceleration and the term $g = GM/R^2$ is known as the gravitational acceleration or, simply, *gravity*. The weight of the mass is given by mg.

On such an Earth, gravity would be constant. However, the Earth's ellipsoidal shape, rotation, irregular surface relief and internal mass distribution cause gravity to vary over its surface.

The gravitational field is most usefully defined in terms of the *gravitational potential* U:

$$U = \frac{GM}{r} \tag{6.3}$$

Whereas the gravitational acceleration g is a vector quantity, having both magnitude and direction (vertically downwards), the gravitational potential U is a scalar, having magnitude only. The first derivative of U in any direction gives the component of gravity in that direction. Consequently, a potential field approach provides computational flexibility. Equipotential surfaces can be defined on which U is constant. The sea-level surface, or *geoid*, is the most easily recognized equipotential surface, which is everywhere horizontal, that is, at right angles to the direction of gravity.

6.3 Units of gravity

The mean value of gravity at the Earth's surface is about $9.8\,\mathrm{m\,s^{-2}}$. Variations in gravity caused by density variations in the subsurface are of the order of $100\,\mu\mathrm{m\,s^{-2}}$. This unit of the micrometre per second per second is referred to as the *gravity unit* (gu). In gravity surveys on land an accuracy of ± 0.1 gu is readily attainable, corresponding to about one hundred millionth of the normal gravitational field. At sea the accuracy obtainable is considerably less, about ± 10 gu. The c.g.s. unit of gravity is the *milligal* ($1\,\mathrm{mgal} = 10^{-3}\,\mathrm{gal} = 10^{-3}\,\mathrm{cm\,s^{-2}}$), equivalent to 10 gu.

6.4 Measurement of gravity

Since gravity is an acceleration, its measurement should simply involve determinations of length and time. However, such apparently simple measurements are not easily achievable at the precision and accuracy required in gravity surveying.

The measurement of an absolute value of gravity is difficult and requires complex apparatus and a lengthy period of observation. Such measurement is classically made using large pendulums or falling body techniques (see e.g. Nettleton 1976, Whitcomb 1987), which can be made with a precision of 0.01 gu. Instruments for measuring absolute gravity in the field were originally bulky, expensive and slow to read (see e.g. Sakuma 1986). A new generation of absolute reading instruments (Brown *et al.* 1999) is now under development which does not suffer from these drawbacks and may well be in more general use in years to come.

The measurement of relative values of gravity, that is, the differences of gravity between locations, is simpler and is the standard procedure in gravity surveying. Absolute gravity values at survey stations may be obtained by reference to the International Gravity Standardization Network (IGSN) of 1971 (Morelli *et al.* 1971), a network of stations at which the absolute values of gravity have been determined by reference to sites of absolute gravity measurements (see Section 6.7). By using a relative reading instrument to determine the difference in gravity between an IGSN station and a field location the absolute value of gravity at that location can be determined.

Previous generations of relative reading instruments were based on small pendulums or the oscillation of torsion fibres and, although portable, took considerable time to read. Modern instruments capable of rapid gravity measurements are known as *gravity meters* or *gravimeters*.

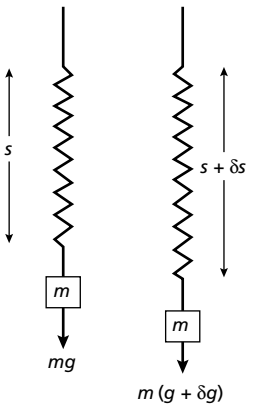

Fig. 6.1 Principle of stable gravimeter operation.

Gravimeters are basically spring balances carrying a constant mass. Variations in the weight of the mass caused by variations in gravity cause the length of the spring to vary and give a measure of the change in gravity. In Fig. 6.1 a spring of initial length s has been stretched by an amount δs as a result of an increase in gravity δg increasing the weight of the suspended mass m. The extension of the spring is proportional to the extending force (Hooke's Law), thus

$$m\delta g = k\delta s$$

and

$$\delta s = \frac{m}{k}\delta g \tag{6.4}$$

where k is the elastic spring constant.

δs must be measured to a precision of $1 : 10^8$ in instruments suitable for gravity surveying on land. Although a large mass and a weak spring would increase the ratio m/k and, hence, the sensitivity of the instrument, in practice this would make the system liable to collapse. Consequently, some form of optical, mechanical or electronic amplification of the extension is required in practice.

The necessity for the spring to serve a dual function, namely to support the mass and to act as the measuring device, severely restricted the sensitivity of early gravimeters, known as stable or static gravimeters. This

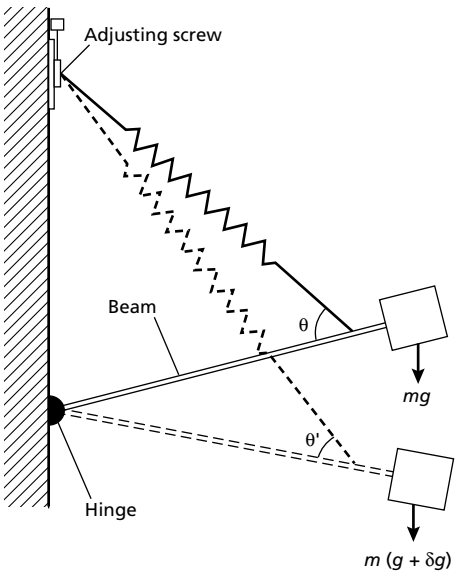

Fig. 6.2 Principle of the LaCoste and Romberg gravimeter.

problem is overcome in modern meters (unstable or astatic) which employ an additional force that acts in the same sense as the extension (or contraction) of the spring and consequently amplifies the movement directly.

An example of an unstable instrument is the LaCoste and Romberg gravimeter. The meter consists of a hinged beam, carrying a mass, supported by a spring attached immediately above the hinge (Fig. 6.2). The magnitude of the moment exerted by the spring on the beam is dependent upon the extension of the spring and the sine of the angle θ. If gravity increases, the beam is depressed and the spring further extended. Although the restoring force of the spring is increased, the angle θ is decreased to θ'. By suitable design of the spring and beam geometry the magnitude of the increase of restoring moment with increasing gravity can be made as small as desired. With ordinary springs the working range of such an instrument would be very small. However, by making use of a 'zero-length' spring which is pretensioned during manufacture so that the restoring force is proportional to the physical length of the spring rather than its extension, instruments can be fashioned with a very sensitive response over a wide range. The instrument is read by restoring the beam to the horizontal by altering the vertical location of the spring attachment with a micrometer screw. Thermal effects are removed by a battery-powered thermostatting system. The range of the instrument is 50 000 gu.

The other unstable instrument in common use is the Worden-type gravimeter. The necessary instability is provided by a similar mechanical arrangement, but in this case the beam is supported by two springs. The first of these springs acts as the measuring device, while the second alters the level of the 2000 gu reading range of the instrument. In certain specialized forms of this instrument the second spring is also calibrated, so that the overall reading range is similar to that of the LaCoste and Romberg gravimeter. Thermal effects are normally minimized by the use of quartz components and a bimetallic beam which compensates automatically for temperature changes. Consequently, no thermostatting is required and it is simply necessary to house the instrument in an evacuated flask. The restricted range of normal forms of the instrument, however, makes it unsuitable for intercontinental gravity ties or surveys in areas where gravity variation is extreme.

Gravimeters for general surveying use are capable of registering changes in gravity with an accuracy of 0.1 gu. A new generation of more efficient zero-length springs has been developed. Microprocessor-controlled instruments are now available which are, within limits, self-levelling, and which allow observations to be made rapidly. Also available for more specialized surveys (Section 6.12) are gravimeters capable of detecting gravity changes as small as 1 microgal (10^{-8} m s^{-2}).

A shortcoming of gravimeters is the phenomenon of *drift*. This refers to a gradual change in reading with time, observable when the instrument is left at a fixed location. Drift results from the imperfect elasticity of the springs, which undergo anelastic creep with time. Drift can also result from temperature variations which, unless counteracted in some way, cause expansion or contraction of the measuring system and thus give rise to variations in measurements that are unrelated to changes in gravity. Drift is monitored by repeated meter readings at a fixed location throughout the day.

Gravity can be measured at discrete locations at sea using a remote-controlled land gravimeter, housed in a waterproof container, which is lowered over the side of the ship and, by remote operation, levelled and read on the sea bed. Measurements of comparable quality to readings on land can be obtained in this way, and the method has been used with success in relatively shallow waters. The disadvantage of the method is that the meter has to be lowered to the sea bed for each reading so that the rate of surveying is very slow. Moreover, in strong

tidal currents, the survey ship needs to be anchored to keep it on station while the gravimeter is on the sea bed.

Gravity measurements can be made continuously at sea using a gravimeter modified for use on ships. Such instruments are known as shipborne, or shipboard, meters. The accuracy of measurements with a shipborne meter is considerably reduced compared to measurements on land because of the severe vertical and horizontal accelerations imposed on the shipborne meter by sea waves and the ship's motion. These external accelerations can cause variations in measured gravity of up to 10^6 gu and represent high-amplitude noise from which a signal of much smaller gravity variations must be extracted. The effects of horizontal accelerations produced by waves, yawing of the ship and changes in its speed and heading can be largely eliminated by mounting the meter on a gyrostabilized, horizontal platform, so that the meter only responds to vertical accelerations. Deviations of the platform from the horizontal produce *off-levelling errors* which are normally less than 10 gu. External vertical accelerations resulting from wave motions cannot be distinguished from gravity but their effect can be diminished by heavily damping the suspension system and by averaging the reading over an interval considerably longer than the maximum period of the wave motions (about 8 s). As the ship oscillates vertically above and below the plane of the mean sea surface, the wave accelerations are equally negative and positive and are effectively removed by averaging over a few minutes. The operation is essentially low-pass filtering in which accelerations with periods of less than 1–5 min are rejected.

With shipborne meters employing a beam-supported sensor, such as the LaCoste and Romberg instrument, a further complication arises due to the influence of horizontal accelerations. The beam of the meter oscillates under the influence of the varying vertical accelerations caused by the ship's motions. When the beam is tilted out of the horizontal it will be further displaced by the turning force associated with any horizontal acceleration. For certain phase relationships between the vertical and horizontal components of motion of the ship, the horizontal accelerations may cause beam displacements that do not average out with time. Consider an example where the position of a meter in space describes a circular motion under the influence of sea waves (Fig. 6.3). At time t_1, as shown in Fig. 6.3, the ship is moving down, displacing the beam upwards, and the horizontal component of motion is to the right, inducing an anticlockwise torque that decreases the upward displacement of the beam. At a slightly later time t_3 the ship is moving up, displacing the beam down, and the horizontal motion is to the left, again inducing an anticlockwise torque which, now, increases the downward displacement of the beam. In such a case, the overall effect of the horizontal accelerations is to produce a systematic error in the beam position. This effect is known as *cross-coupling*, and its magnitude is dependent on the damping characteristics of the meter and the amplitude and phase relationships of the horizontal and vertical motions. It leads to an error known as the *cross-coupling error* in the measured gravity value. In general, the cross-coupling error is small or negligible in good weather conditions but can become very large in high seas. Cross-coupling errors are corrected directly from the outputs of two horizontal accelerometers mounted on the stabilized platform.

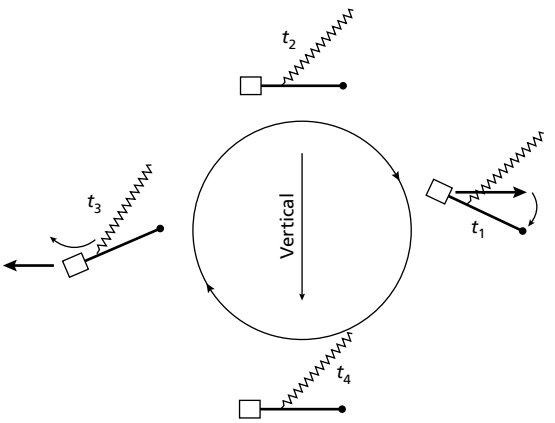

Fig. 6.3 Cross-coupling in a shipborne gravimeter.

The inability to compensate fully for extraneous accelerations reduces the accuracy of these shipborne measurements to 10 gu at best, the actual amount depending on prevailing sea conditions. Instrumental drift monitoring is also less precise as base ties are, of necessity, usually many days apart.

Cross-coupling is one of the major sources of error in measurements of gravity at sea made with instruments utilizing a beam-supported mass, and arises because of the directional nature of the system. No cross-coupling would occur if the sensor were symmetric about a vertical axis, and since the late 1960s new marine meters utilizing this feature have been developed.

The *vibrating string accelerometer* (Bowin *et al.* 1972) is based on the principle that the resonant frequency of a short, vertical string from which a mass is suspended is

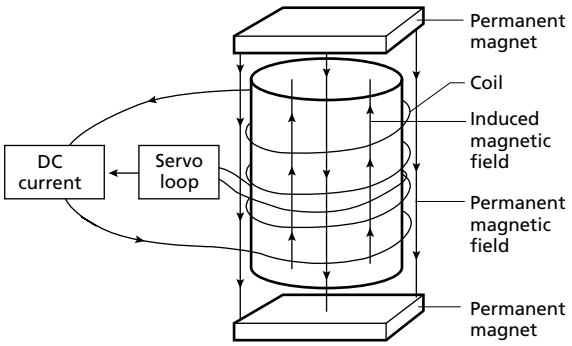

Fig. 6.4 Principle of the accelerometer unit of the Bell marine gravimeter. (After Bell & Watts 1986.)

proportional to the square root of gravity. Changes in this frequency provide a measure of changes in gravity. Gravimeters based on this mechanism have never found much favour because of relatively low reported accuracies and erratic drift.

The most successful axially symmetric instrument to date is the *Bell gravimeter* (Bell & Watts 1986). The sensing element of the meter is the accelerometer shown in Fig. 6.4 which is mounted on a stable platform. The accelerometer, which is about 34 mm high and 23 mm in diameter, consists of a mass, wrapped in a coil, which is constrained to move only vertically between two permanent magnets. A DC current passed through the coil causes the mass to act as a magnet. In the null position, the weight of the mass is balanced by the forces exerted by the permanent magnets. When the mass moves vertically in response to a change in gravity or wave accelerations, the motion is detected by a servo loop which regulates the current in the coil, changing its magnetic moment so that it is driven back to the null position. The varying current is then a measure of changes in the vertical accelerations experienced by the sensor. As with beam-type meters, a weighted average filter is applied to the output in order to separate gravity changes from wave-generated accelerations.

Drift rates of the Bell gravimeter are low and uniform, and it has been demonstrated that the instrument is accurate to just a few gravity units, and is capable of discriminating anomalies with wavelengths of 1–2 km. This accuracy and resolution is considerably greater than that of earlier instruments, and it is anticipated that much smaller gravity anomalies will be detected than was previously possible. The factor preventing more widespread deployment of the meter is its large cost.

The measurement of gravity from aircraft is complex because of the large possible errors in applying corrections. Eötvös corrections (Section 6.8.5) may be as great as 16 000 gu at a speed of 200 knots, a 1% error in velocity or heading producing maximum errors of 180 gu and 250 gu, respectively. Vertical accelerations associated with the aircraft's motion with periods longer than the instrumental averaging time cannot readily be corrected. In spite of these difficulties, tests undertaken in small aircraft (Halpenny & Darbha 1995) equipped with radar altimeters and GPS navigation have achieved results which differ from those obtained with underwater meters by an average of −2 gu and standard deviation 27 gu. Bell *et al.* (1999) describe a more modern set-up for airborne gravity surveying, which is now in use commercially. A system is also available for use with a helicopter (Seigel & McConnell 1998) in which the gravimeter is lowered to the ground by a cable, levelled and read remotely, so that measurements can be made where landing the aircraft is impossible.

The calibration constants of gravimeters may vary with time and should be checked periodically. The most common procedure is to take readings at two or more locations where absolute or relative values of gravity are known. In calibrating Worden-type meters, these readings would be taken for several settings of the coarse adjusting screw so that the calibration constant is checked over as much of the full range of the instrument as possible. Such a procedure cannot be adopted for the LaCoste and Romberg gravimeter, where each different dial range has its own calibration constant. In this case checking can be accomplished by taking readings at different inclinations of the gravimeter on a tilt table, a task usually entrusted to the instrument's manufacturer.

6.5 Gravity anomalies

Gravimeters effectively respond only to the vertical component of the gravitational attraction of an anomalous mass. Consider the gravitational effect of an anomalous mass δg, with horizontal and vertical components δg_x and δg_z, respectively, on the local gravity field g and its representation on a vector diagram (Fig. 6.5).

Solving the rectangle of forces gives

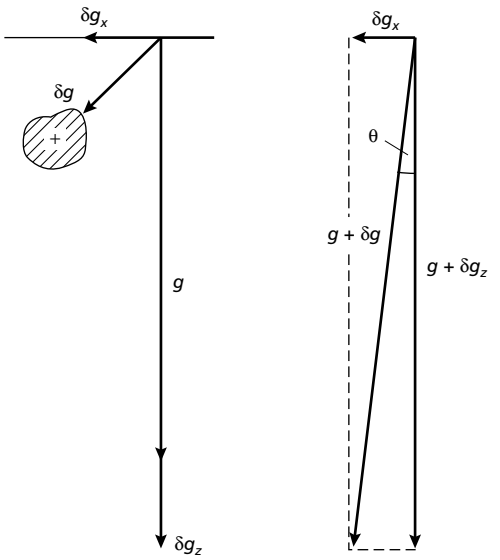

Fig. 6.5 Relationship between the gravitational field and the components of the gravity anomaly of a small mass.

$$g + \delta g = \sqrt{\left((g + \delta g_z)^2 + \delta g_x{}^2\right)}$$
$$= \sqrt{\left(g^2 + 2g\delta g_z + \delta g_z{}^2 + \delta g_x{}^2\right)}$$

Terms in δ^2 are insignificantly small and can thus be ignored. Binomial expansion of the equation then gives

$$g + \delta g \approx g + \delta g_z$$

so that

$$\delta g \approx \delta g_z$$

Consequently, measured perturbations in gravity effectively correspond to the vertical component of the attraction of the causative body. The local deflection of the vertical θ is given by

$$\theta = \tan^{-1}\left(\frac{\delta g_x}{g}\right) \tag{6.5}$$

and since $\delta g_z \ll g$, θ is usually insignificant. Very large mass anomalies such as mountain ranges can, however, produce measurable local vertical deflections.

6.6 Gravity anomalies of simple-shaped bodies

Consider the gravitational attraction of a point mass m at a distance r from the mass (Fig. 6.6). The gravitational attraction Δg_r in the direction of the mass is given by

$$\Delta g_r = \frac{Gm}{r^2} \text{ from Newton's Law.}$$

Since only the vertical component of the attraction Δg_z is measured, the gravity anomaly Δg caused by the mass is

$$\Delta g = \frac{Gm}{r^2}\cos\theta$$

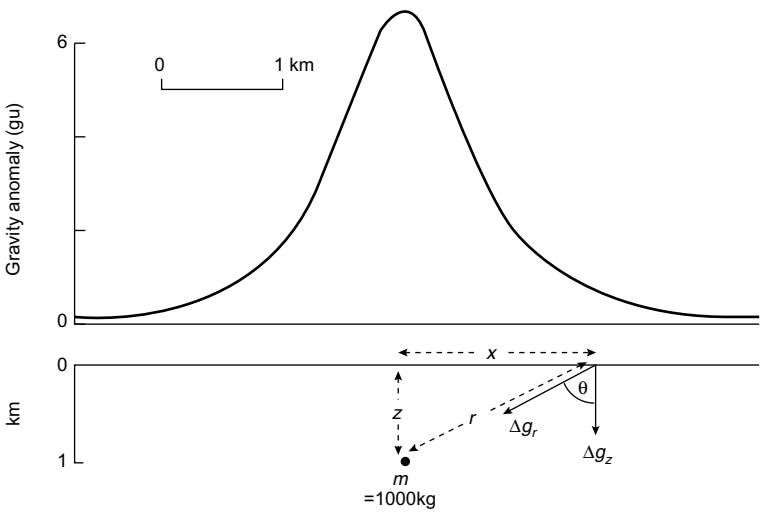

Fig. 6.6 The gravity anomaly of a point mass or sphere.

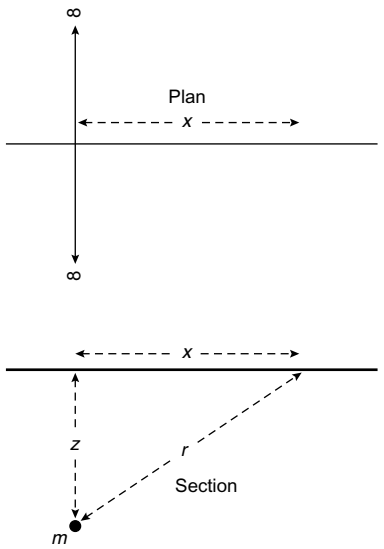

Fig. 6.7 Coordinates describing an infinite horizontal line mass.

or

$$\Delta g = \frac{Gmz}{r^3} \tag{6.6}$$

Since a sphere acts as though its mass were concentrated at its centre, equation (6.6) also corresponds to the gravity anomaly of a sphere whose centre lies at a depth z.

Equation (6.6) can be used to build up the gravity anomaly of many simple geometric shapes by constructing them from a suite of small elements which correspond to point masses, and then summing (integrating) the attractions of these elements to derive the anomaly of the whole body.

Integration of equation (6.6) in a horizontal direction provides the equation for a line mass (Fig. 6.7) extending to infinity in this direction

$$\Delta g = \frac{2Gmz}{r^2} \tag{6.7}$$

Equation (6.7) also represents the anomaly of a horizontal cylinder, whose mass acts as though it is concentrated along its axis.

Integration in the second horizontal direction provides the gravity anomaly of an infinite horizontal sheet, and a further integration in the vertical direction between fixed limits provides the anomaly of an infinite horizontal slab

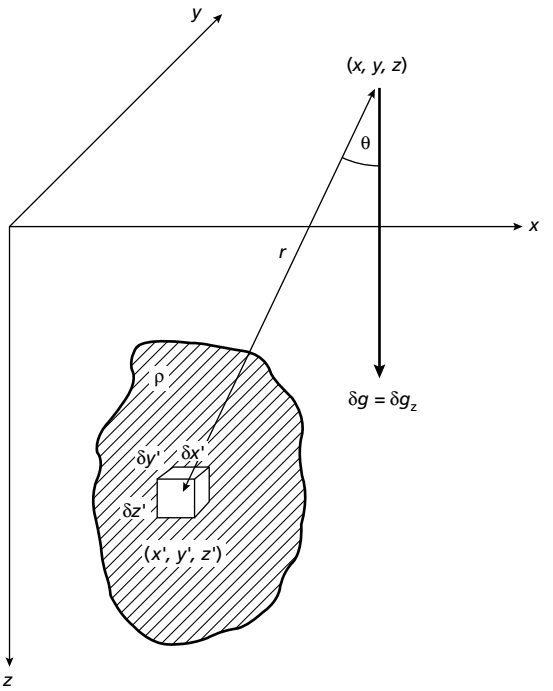

Fig. 6.8 The gravity anomaly of an element of a mass of irregular shape.

$$\Delta g = 2\pi G\rho t \tag{6.8}$$

where ρ is the density of the slab and t its thickness. Note that this attraction is independent of both the location of the observation point and the depth of the slab.

A similar series of integrations, this time between fixed limits, can be used to determine the anomaly of a right rectangular prism.

In general, the gravity anomaly of a body of *any* shape can be determined by summing the attractions of all the mass elements which make up the body. Consider a small prismatic element of such a body of density ρ, located at x', y', z', with sides of length $\delta x'$, $\delta y'$, $\delta z'$ (Fig. 6.8). The mass δm of this element is given by

$$\delta m = \rho\, \delta x'\, \delta y'\, \delta z'$$

Consequently, its attraction δg at a point outside the body (x, y, z), a distance r from the element, is derived from equation (6.6):

$$\delta g = G\rho \frac{(z' - z)}{r^3} \delta x' \delta y' \delta z'$$

The anomaly of the whole body Δg is then found by summing all such elements which make up the body

$$\Delta g = \Sigma\Sigma\Sigma G\rho \frac{(z' - z)}{r^3} \delta x' \delta y' \delta z' \qquad (6.9)$$

If $\delta x'$, $\delta y'$ and $\delta z'$ are allowed to approach zero, then

$$\Delta g = \int\int\int G\rho \frac{(z' - z)}{r^3} \mathrm{d}x' \, \mathrm{d}y' \, \mathrm{d}z' \qquad (6.10)$$

where

$$r = \sqrt{(x' - x)^2 + (y' - y)^2 + (z' - z)^2}$$

As shown before, the attraction of bodies of regular geometry can be determined by integrating equation (6.10) analytically. The anomalies of irregularly shaped bodies are calculated by numerical integration using equations of the form of equation (6.9).

6.7 Gravity surveying

The station spacing used in a gravity survey may vary from a few metres in the case of detailed mineral or geotechnical surveys to several kilometres in regional reconnaissance surveys. The station density should be greatest where the gravity field is changing most rapidly, as accurate measurement of gravity gradients is critical to subsequent interpretation. If absolute gravity values are required in order to interface the results with other gravity surveys, at least one easily accessible base station must be available where the absolute value of gravity is known. If the location of the nearest IGSN station is inconvenient, a gravimeter can be used to establish a local base by measuring the difference in gravity between the IGSN station and the local base. Because of instrumental drift this cannot be accomplished directly and a procedure known as *looping* is adopted. A series of alternate readings at recorded times is made at the two stations and drift curves constructed for each (Fig. 6.9). The differences in ordinate measurements (Δg_{1-4}) for the two stations then may be averaged to give a measure of the drift-corrected gravity difference.

During a gravity survey the gravimeter is read at a base station at a frequency dependent on the drift characteristics of the instrument. At each survey station, location, time, elevation/water depth and gravimeter reading are recorded.

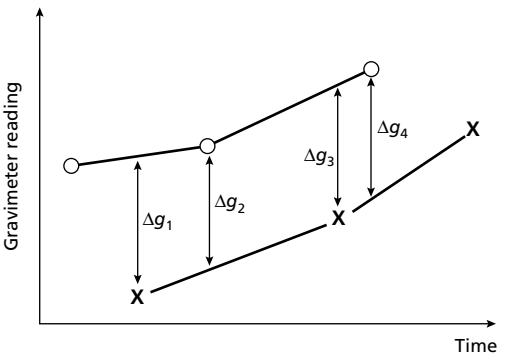

Fig. 6.9 The principle of looping. Crosses and circles represent alternate gravimeter readings taken at two base stations. The vertical separations between the drift curves for the two stations (Δg_{1-4}) provide an estimate of the gravity difference between them.

In order to obtain a reduced gravity value accurate to ± 1 gu, the reduction procedure described in the following section indicates that the gravimeter must be read to a precision of ± 0.1 gu, the latitude of the station must be known to ± 10 m and the elevation of the station must be known to ± 10 mm. The latitude of the station must consequently be determined from maps at a scale of 1 : 10 000 or smaller, or by the use of electronic position-fixing systems. Uncertainties in the elevations of gravity stations probably account for the greatest errors in reduced gravity values on land; at sea, water depths are easily determined with a precision depth recorder to an accuracy consistent with the gravity measurements. In well-surveyed land areas, the density of accurately-determined elevations at bench marks is normally sufficiently high that gravity stations can be sited at bench marks or connected to them by levelling surveys. Reconnaissance gravity surveys of less well-mapped areas require some form of independent elevation determination. Many such areas have been surveyed using aneroid altimeters. The accuracy of heights determined by such instruments is dependent upon the prevailing climatic conditions and is of the order of 1–5 m, leading to a relatively large uncertainty in the elevation corrections applied to the measured gravity values. The optimal equipment at present is the global positioning system (GPS) (Davis *et al.* 1989), whose constellation of 24 satellites is now complete and an unadulterated signal is broadcast. Signals from these can be monitored by a small, inexpensive receiver. Use of differential GPS, that is, the comparison between GPS signals between a base

set at a known elevation and a mobile field set, can provide elevations to an accuracy of some 25 mm.

6.8 Gravity reduction

Before the results of a gravity survey can be interpreted it is necessary to correct for all variations in the Earth's gravitational field which do not result from the differences of density in the underlying rocks. This process is known as *gravity reduction* (LaFehr 1991) or *reduction to the geoid*, as sea-level is usually the most convenient datum level.

6.8.1 Drift correction

Correction for instrumental drift is based on repeated readings at a base station at recorded times throughout the day. The meter reading is plotted against time (Fig. 6.10) and drift is assumed to be linear between consecutive base readings. The drift correction at time t is d, which is subtracted from the observed value.

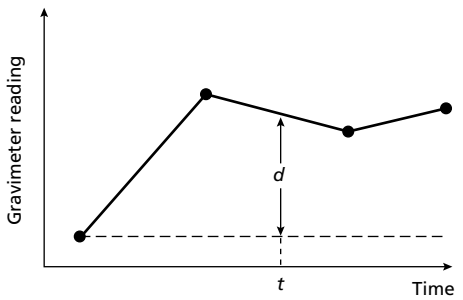

Fig. 6.10 A gravimeter drift curve constructed from repeated readings at a fixed location. The drift correction to be subtracted for a reading taken at time t is d.

After drift correction the difference in gravity between an observation point and the base is found by multiplication of the difference in meter reading by the calibration factor of the gravimeter. Knowing this difference in gravity, the absolute gravity at the observation point g_{obs} can be computed from the known value of gravity at the base. Alternatively, readings can be related to an arbitrary datum, but this practice is not desirable as the results from different surveys cannot then be tied together.

6.8.2 Latitude correction

Gravity varies with latitude because of the non-spherical shape of the Earth and because the angular velocity of a point on the Earth's surface decreases from a maximum at the equator to zero at the poles (Fig. 6.11(a)). The centripetal acceleration generated by this rotation has a negative radial component that consequently causes gravity to decrease from pole to equator. The true shape of the Earth is an oblate spheroid or polar flattened ellipsoid (Fig. 6.11(b)) whose difference in equatorial and polar radii is some 21 km. Consequently, points near the equator are farther from the centre of mass of the Earth than those near the poles, causing gravity to increase from the equator to the poles. The amplitude of this effect is reduced by the differing subsurface mass distributions resulting from the equatorial bulge, the mass underlying equatorial regions being greater than that underlying polar regions.

The net effect of these various factors is that gravity at

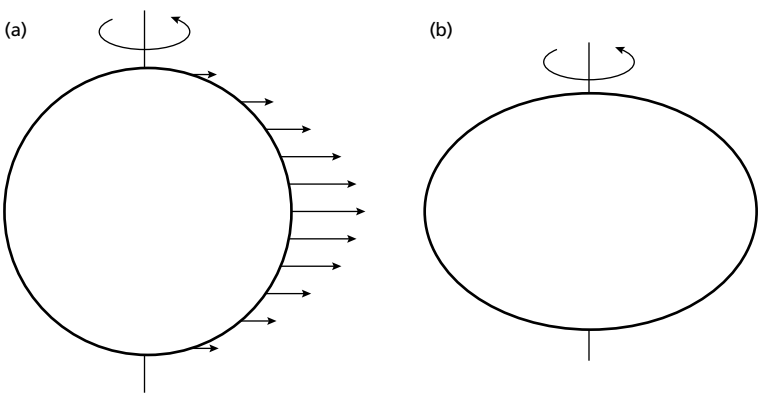

Fig. 6.11 (a) The variation in angular velocity with latitude around the Earth represented by vectors whose lengths are proportional to angular velocity. (b) An exaggerated representation of the shape of the Earth. The true shape of this oblate ellipsoid of revolution results in a difference in equatorial and polar radii of some 21 km.

the poles exceeds gravity at the equator by some 51 860 gu, with the north–south gravity gradient at latitude ϕ being $8.12 \sin 2\phi$ gu km^{-1}.

Clairaut's formula relates gravity to latitude on the reference spheroid according to an equation of the form

$$g_\phi = g_0(1 + k_1 \sin^2 \phi - k_2 \sin^2 2\phi) \qquad (6.11)$$

where g_ϕ is the predicted value of gravity at latitude ϕ, g_0 is the value of gravity at the equator and k_1, k_2 are constants dependent on the shape and speed of rotation of the Earth. Equation (6.11) is, in fact, an approximation of an infinite series. The values of g_0, k_1 and k_2 in current use define the International Gravity Formula 1967 ($g_0 = 9\,780\,318$ gu, $k_1 = 0.0053024$, $k_2 = 0.0000059$; IAG 1971). Prior to 1967 less accurate constants were employed in the International Gravity Formula (1930). Results deduced using the earlier formula must be modified before incorporation into survey data reduced using the Gravity Formula 1967 by using the relationship $g_\phi(1967) - g_\phi(1930) = (136 \sin^2 \phi - 172)$ gu.

An alternative, more accurate, representation of the Gravity Formula 1967 (Mittermayer 1969), in which the constants are adjusted so as to minimize errors resulting from the truncation of the series, is

$$g_\phi = 9\,780\,318.5\,(1 + 0.005278895 \sin^2 \phi + 0.000023462 \sin^4 \phi) \text{ gu}$$

This form, however, is less suitable if the survey results are to incorporate pre-1967 data made compatible with the Gravity Formula 1967 using the above relationship.

The value g_ϕ gives the predicted value of gravity at sea-level at any point on the Earth's surface and is subtracted from the observed gravity to correct for latitude variation.

6.8.3 Elevation corrections

Correction for the differing elevations of gravity stations is made in three parts. The free-air correction (FAC) corrects for the decrease in gravity with height in free air resulting from increased distance from the centre of the Earth, according to Newton's Law. To reduce to datum an observation taken at height h (Fig. 6.12(a)),

$$\text{FAC} = 3.086h \text{ gu } (h \text{ in metres})$$

The FAC is positive for an observation point above datum to correct for the decrease in gravity with elevation.

The free-air correction accounts solely for variation in the distance of the observation point from the centre of the Earth; no account is taken of the gravitational effect of the rock present between the observation point and datum. The *Bouguer correction* (BC) removes this effect by approximating the rock layer beneath the observation point to an infinite horizontal slab with a thickness equal to the elevation of the observation above datum (Fig. 6.12(b)). If ρ is the density of the rock, from equation (6.8)

$$\text{BC} = 2\pi G\rho h = 0.4191\rho h \text{ gu}$$
$$(h \text{ in metres}, \rho \text{ in Mg m}^{-3})$$

On land the Bouguer correction must be subtracted, as the gravitational attraction of the rock between observation point and datum must be removed from the observed gravity value. The Bouguer correction of sea surface observations is positive to account for the lack of rock between surface and sea bed. The correction is equivalent to the replacement of the water layer by material of a specified rock density ρ_r. In this case

$$\text{BC} = 2\pi G(\rho_r - \rho_w)z$$

where z is the water depth and ρ_w the density of water.

The free-air and Bouguer corrections are often applied together as the *combined elevation correction*.

The Bouguer correction makes the assumption that the topography around the gravity station is flat. This is

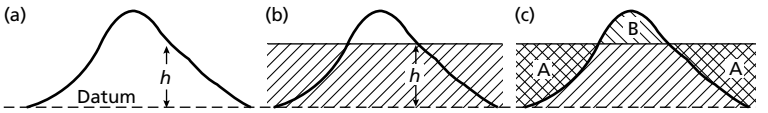

Fig. 6.12 (a) The free-air correction for an observation at a height h above datum. (b) The Bouguer correction. The shaded region corresponds to a slab of rock of thickness h extending to infinity in both horizontal directions. (c) The terrain correction.

rarely the case and a further correction, the *terrain correction* (TC), must be made to account for topographic relief in the vicinity of the gravity station. This correction is always positive as may be appreciated from consideration of Fig. 6.12(c). The regions designated A form part of the Bouguer correction slab although they do not consist of rock. Consequently, the Bouguer correction has overcorrected for these areas and their effect must be restored by a positive terrain correction. Region B consists of rock material that has been excluded from the Bouguer correction. It exerts an upward attraction at the observation point causing gravity to decrease. Its attraction must thus be corrected by a positive terrain correction.

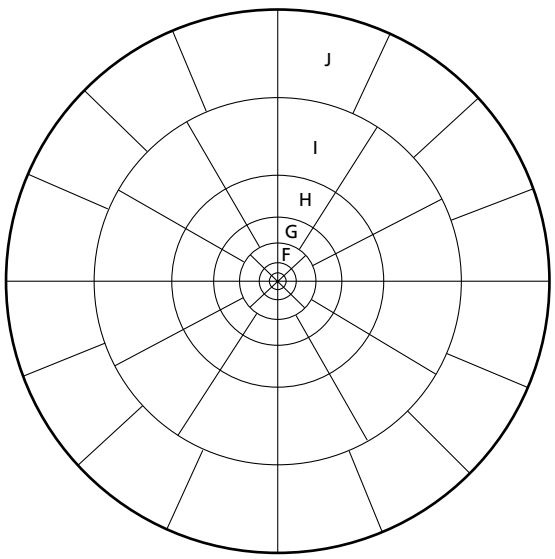

Fig. 6.13 A typical graticule used in the calculation of terrain corrections. A series of such graticules with zones varying in radius from 2 m to 21.9 km is used with topographic maps of varying scale.

Classically, terrain corrections are applied using a circular graticule known, after its inventor, as a Hammer chart (Fig. 6.13), divided by radial and concentric lines into a large number of compartments. The outermost zone extends to almost 22 km, beyond which topographic effects are usually negligible. The graticule is laid on a topographic map with its centre on the gravity station and the average topographic elevation of each compartment is determined. The elevation of the gravity station is subtracted from these values, and the gravitational effect of each compartment is determined by reference to tables constructed using the formula for the gravitational effect of a sector of a vertical cylinder at its axis. The terrain correction is then computed by summing the gravitational contribution of all compartments. Table 6.1 shows the method of computation. Such operations are time consuming as the topography of over 130 compartments has to be averaged for each station, but terrain correction is the one operation in gravity reduction that cannot be fully automated. Labour can be reduced by averaging topography within a rectangular grid. Only a single digitization is required as the topographic effects may be calculated at any point within the grid by summing the effects of the right rectangular prisms defined by the grid squares and their elevation difference with the gravity station. This operation can effectively correct for the topography of areas distant

Table 6.1 Terrain corrections.

Zone	r_1	r_2	n	Zone	r_1	r_2	n
B	2.0	16.6	4	H	1529.4	2614.4	12
C	16.6	53.3	6	I	2614.4	4468.8	12
D	53.3	170.1	6	J	4468.8	6652.2	16
E	170.1	390.1	8	K	6652.2	9902.5	16
F	390.1	894.8	8	L	9902.5	14740.9	16
G	894.8	1529.4	12	M	14740.9	21943.3	16

$$T = 0.4191\frac{\rho}{n}\left(r_2 - r_1 + \sqrt{r_1^2 + z^2} - \sqrt{r_2^2 + z^2}\right)$$

where T = terrain correction of compartment (gu); ρ = Bouguer correction density ($Mg\,m^{-3}$); n = number of compartments in zone; r_1 = inner radius of zone (m); r_2 = outer radius of zone (m); and z = modulus of elevation difference between observation point and mean elevation of compartment (m).

from the gravity station and can be readily computerized. Such an approach is likely to be increasingly adopted as digital elevation models for large regions become available (Cogbill 1990). Correction for inner zones, however, must still be performed manually as any reasonable digitization scheme for a complete survey area and its environs must employ a sampling interval that is too large to provide an accurate representation of the terrain close to the station.

Terrain effects are low in areas of subdued topography, rarely exceeding 10 gu in flat-lying areas. In areas of rugged topography terrain effects are considerably greater, being at a maximum in steep-sided valleys, at the base or top of cliffs and at the summits of mountains.

Where terrain effects are considerably less than the desired accuracy of a survey, the terrain correction may be ignored. Sprenke (1989) provides a means of assessing the distance to which terrain corrections are necessary. However, the usual necessity for this correction accounts for the bulk of time spent on gravity reduction and is thus a major contributor to the cost of a gravity survey.

6.8.4 Tidal correction

Gravity measured at a fixed location varies with time because of periodic variation in the gravitational effects of the Sun and Moon associated with their orbital motions, and correction must be made for this variation in a high-precision survey. In spite of its much smaller mass, the gravitational attraction of the Moon is larger than that of the Sun because of its proximity. Also, these gravitational effects cause the shape of the solid Earth to vary in much the same way that the celestial attractions cause tides in the sea. These *solid Earth tides* are considerably smaller than oceanic tides and lag farther behind the lunar motion. They cause the elevation of an observation point to be altered by a few centimetres and thus vary its distance from the centre of mass of the Earth. The periodic gravity variations caused by the combined effects of Sun and Moon are known as *tidal variations*. They have a maximum amplitude of some 3 gu and a minimum period of about 12 h.

If a gravimeter with a relatively high drift rate is used, base ties are made at an interval much smaller than the minimum Earth tide period and the tidal variations are automatically removed during the drift correction. If a meter with a low drift rate is employed, base ties are normally made only at the start and end of the day so that the tidal variation has undergone a full cycle. In such a case, a separate tidal correction may need to be made. The tidal effects are predictable and can be computed by a small computer program.

6.8.5 Eötvös correction

The Eötvös correction (EC) is applied to gravity measurements taken on a moving vehicle such as a ship or an aircraft. Depending on the direction of travel, vehicular motion will generate a centripetal acceleration which either reinforces or opposes gravity. The correction required is

$$\mathrm{EC} = 75.03V \sin\alpha \cos\phi + 0.04154V^2 \text{ gu}$$

where V is the speed of the vehicle in knots, α the heading and ϕ the latitude of the observation. In mid-latitudes the Eötvös correction is about +75 gu for each knot of E to W motion so that speed and heading must be accurately known.

6.8.6 Free-air and Bouguer anomalies

The *free-air anomaly* (FAA) and *Bouguer anomaly* (BA) may now be defined

$$\mathrm{FAA} = g_{\mathrm{obs}} - g_{\phi} + \mathrm{FAC}\ (\pm\mathrm{EC}) \tag{6.12}$$

$$\mathrm{BA} = g_{\mathrm{obs}} - g_{\phi} + \mathrm{FAC} \pm \mathrm{BC} + \mathrm{TC}\ (\pm\mathrm{EC}) \tag{6.13}$$

The Bouguer anomaly forms the basis for the interpretation of gravity data on land. In marine surveys Bouguer anomalies are conventionally computed for inshore and shallow water areas as the Bouguer correction removes the local gravitational effects associated with local changes in water depth. Moreover, the computation of the Bouguer anomaly in such areas allows direct comparison of gravity anomalies offshore and onshore and permits the combination of land and marine data into gravity contour maps. These may be used, for example, in tracing geological features across coastlines. The Bouguer anomaly is not appropriate for deeper water surveys, however, as in such areas the application of a Bouguer correction is an artificial device that leads to very large positive Bouguer anomaly values without significantly enhancing local gravity features of geological origin. Consequently, the free-air anomaly is frequently used for interpretation in such areas. Moreover, the FAA provides a broad assessment of the degree of isostatic compensation of an area (e.g. Bott 1982).

Gravity anomalies are conventionally displayed on

profiles or as contoured (isogal) maps. Interpretation of the latter may be facilitated by utilizing digital image processing techniques similar to those used in the display of remotely sensed data. In particular, colour and shaded relief images may reveal structural features that may not be readily discernible on unprocessed maps (Plate 5.1a). This type of processing is equally appropriate to magnetic anomalies (Plate 5.1b; see for example Lee *et al.* 1990).

6.9 Rock densities

Gravity anomalies result from the difference in density, or *density contrast*, between a body of rock and its surroundings. For a body of density ρ_1 embedded in material of density ρ_2, the density contrast $\Delta\rho$ is given by

$$\Delta\rho = \rho_1 - \rho_2$$

The sign of the density contrast determines the sign of the gravity anomaly.

Rock densities are among the least variable of all geophysical parameters. Most common rock types have densities in the range between 1.60 and 3.20 $Mg\,m^{-3}$. The density of a rock is dependent on both its mineral composition and porosity.

Variation in porosity is the main cause of density variation in sedimentary rocks. Thus, in sedimentary rock sequences, density tends to increase with depth, due to compaction, and with age, due to progressive cementation.

Most igneous and metamorphic rocks have negligible porosity, and composition is the main cause of density variation. Density generally increases as acidity decreases; thus there is a progression of density increase from acid through basic to ultrabasic igneous rock types. Density ranges for common rock types and ores are presented in Table 6.2.

A knowledge of rock density is necessary both for application of the Bouguer and terrain corrections and for the interpretation of gravity anomalies.

Density is commonly determined by direct measurements on rock samples. A sample is weighed in air and in water. The difference in weights provides the volume of the sample and so the dry density can be obtained. If the rock is porous the saturated density may be calculated by following the above procedure after saturating the rock with water. The density value employed in interpretation then depends upon the location of the rock above or below the water table.

Table 6.2 Approximate density ranges ($Mg\,m^{-3}$) of some common rock types and ores.

Alluvium (wet)	1.96–2.00
Clay	1.63–2.60
Shale	2.06–2.66
Sandstone	
Cretaceous	2.05–2.35
Triassic	2.25–2.30
Carboniferous	2.35–2.55
Limestone	2.60–2.80
Chalk	1.94–2.23
Dolomite	2.28–2.90
Halite	2.10–2.40
Granite	2.52–2.75
Granodiorite	2.67–2.79
Anorthosite	2.61–2.75
Basalt	2.70–3.20
Gabbro	2.85–3.12
Gneiss	2.61–2.99
Quartzite	2.60–2.70
Amphibolite	2.79–3.14
Chromite	4.30–4.60
Pyrrhotite	4.50–4.80
Magnetite	4.90–5.20
Pyrite	4.90–5.20
Cassiterite	6.80–7.10
Galena	7.40–7.60

NB. The lower end of the density range quoted in many texts is often unreasonably extended by measurements made on samples affected by physical or chemical weathering.

It should be stressed that the density of any particular rock type can be quite variable. Consequently, it is usually necessary to measure several tens of samples of each particular rock type in order to obtain a reliable mean density and variance.

As well as these direct methods of density determination, there are several indirect (or *in situ*) methods. These usually provide a mean density of a particular rock unit which may be internally quite variable. *In situ* methods do, however, yield valuable information where sampling is hampered by lack of exposure or made impossible because the rocks concerned occur only at depth.

The measurement of gravity at different depths beneath the surface using a special borehole gravimeter (see Section 11.11) or, more commonly, a standard gravimeter in a mineshaft, provides a measure of the mean density of the material between the observation levels. In Fig. 6.14 gravity has been measured at the surface and at a point underground at a depth h immediately below. If g_1 and g_2 are the values of gravity

obtained at the two levels, then, applying free-air and Bouguer corrections, one obtains

$$g_1 - g_2 = 3.086h - 4\pi G\rho h \qquad (6.14)$$

The Bouguer correction is double that employed on the surface as the slab of rock between the observation levels exerts both a downward attraction at the surface location and an upward attraction at the underground location. The density ρ of the medium separating the two observations can then be found from the difference in gravity. Density may also be measured in boreholes using a density (gamma–gamma) logger as discussed in Section 11.7.2.

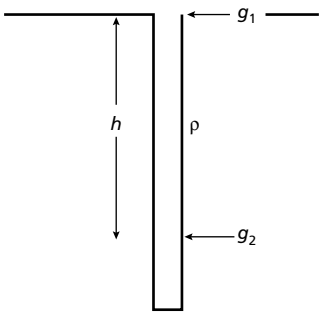

Fig. 6.14 Density determination by subsurface gravity measurements. The measured gravity difference $g_1 - g_2$ over a height difference h can be used to determine the mean density ρ of the rock separating the measurements.

Nettleton's method of density determination involves taking gravity observations over a small isolated topographic prominence. Field data are reduced using a series of different densities for the Bouguer and terrain corrections (Fig. 6.15). The density value that yields a Bouguer anomaly with the least correlation (positive or negative) with the topography is taken to represent the density of the prominence. The method is useful in that no borehole or mineshaft is required, and a mean density of the material forming the prominence is provided. A disadvantage of the method is that isolated relief features may be formed of anomalous materials which are not representative of the area in general.

Density information is also provided from the P-wave velocities of rocks obtained in seismic surveys.

Figure 6.16 shows graphs of the logarithm of P-wave velocity against density for various rock types (Gardner *et al.* 1974), and the best-fitting linear relationship. Other

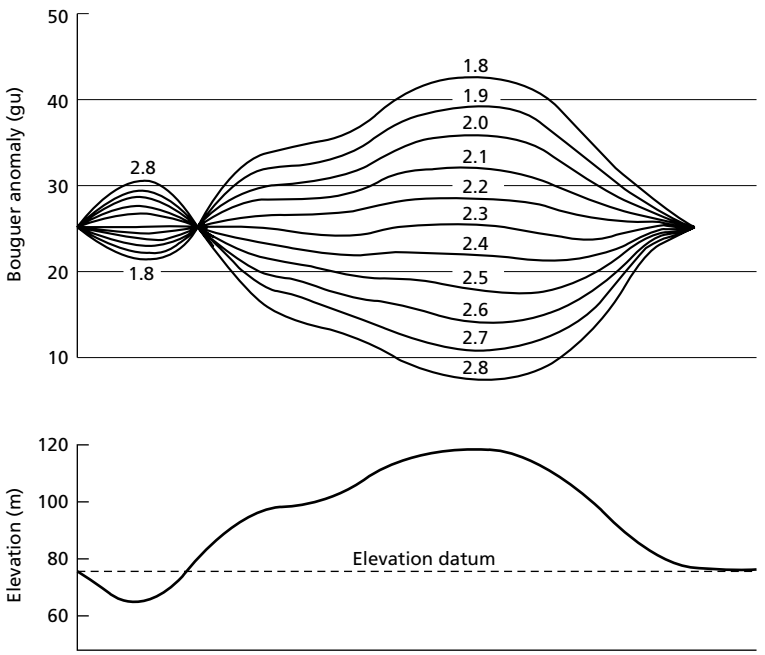

Fig. 6.15 Nettleton's method of density determination over an isolated topographic feature. Gravity reductions have been performed using densities ranging from 1.8 to 2.8 Mg m^{-3} for both Bouguer and terrain corrections. The profile corresponding to a value of 2.3 Mg m^{-3} shows least correlation with topography so this density is taken to represent the density of the feature. (After Dobrin & Savit 1988.)

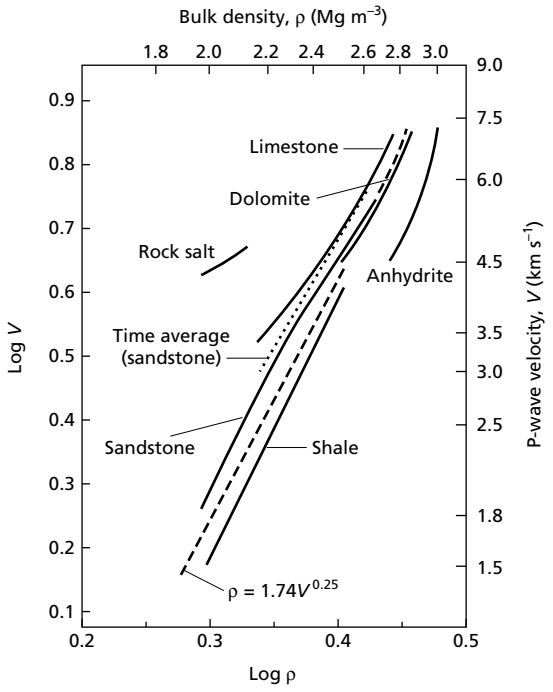

Fig. 6.16 Graphs of the logarithm of P-wave velocity against density for various rock types. Also shown is the best-fitting linear relationship between density and log velocity (after Gardner *et al.* 1974).

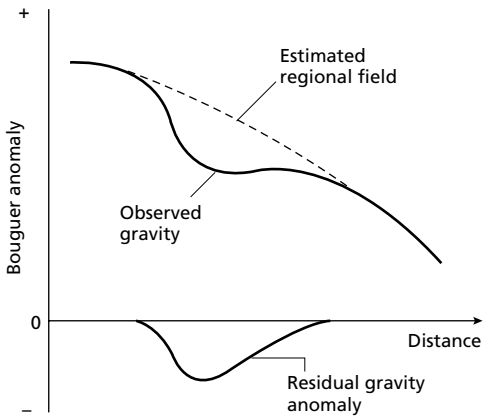

Fig. 6.17 The separation of regional and residual gravity anomalies from the observed Bouguer anomaly.

workers (e.g. Birch 1960, 1961, Christensen & Fountain 1975) have derived similar relationships. The empirical velocity–density curve of Nafe and Drake (1963) indicates that densities estimated from seismic velocities are probably no more accurate than about $\pm 0.10\,\mathrm{Mg\,m^{-3}}$. This, however, is the only method available for the estimation of densities of deeply buried rock units that cannot be sampled directly.

6.10 Interpretation of gravity anomalies

6.10.1 The inverse problem

The interpretation of potential field anomalies (gravity, magnetic and electrical) is inherently ambiguous. The ambiguity arises because any given anomaly could be caused by an infinite number of possible sources. For example, concentric spheres of constant mass but differing density and radius would all produce the same anomaly, since their mass acts as though located at the centre of the sphere. This ambiguity represents the *inverse problem* of potential field interpretation, which states that, although the anomaly of a given body may be calculated uniquely, there are an infinite number of bodies that could give rise to any specified anomaly. An important task in interpretation is to decrease this ambiguity by using all available external constraints on the nature and form of the anomalous body. Such constraints include geological information derived from surface outcrops, boreholes and mines, and from other, complementary, geophysical techniques (see e.g. Lines *et al.* 1988).

6.10.2 Regional fields and residual anomalies

Bouguer anomaly fields are often characterized by a broad, gently varying, regional anomaly on which may be superimposed shorter wavelength local anomalies (Fig. 6.17). Usually in gravity surveying it is the local anomalies that are of prime interest and the first step in interpretation is the removal of the *regional field* to isolate the *residual anomalies*. This may be performed graphically by sketching in a linear or curvilinear field by eye. Such a method is biased by the interpreter, but this is not necessarily disadvantageous as geological knowledge can be incorporated into the selection of the regional field. Several analytical methods of regional field analysis are available and include trend surface analysis (fitting a polynomial to the observed data, see Beltrão *et al.* (1991)) and low-pass filtering (Section 6.12). Such procedures must be used critically as fictitious residual anomalies can sometimes arise when the regional field is

subtracted from the observed data due to the mathematical procedures employed.

It is necessary before carrying out interpretation to differentiate between two-dimensional and three-dimensional anomalies. Two-dimensional anomalies are elongated in one horizontal direction so that the anomaly length in this direction is at least twice the anomaly width. Such anomalies may be interpreted in terms of structures which theoretically extend to infinity in the elongate direction by using profiles at right angles to the strike. Three-dimensional anomalies may have any shape and are considerably more difficult to interpret quantitatively.

Gravity interpretation proceeds via the methods of direct and indirect interpretation.

6.10.3 Direct interpretation

Direct interpretation provides, directly from the gravity anomalies, information on the anomalous body which is largely independent of the true shape of the body. Various methods are discussed below.

Limiting depth

Limiting depth refers to the maximum depth at which the top of a body could lie and still produce an observed gravity anomaly. Gravity anomalies decay with the inverse square of the distance from their source so that anomalies caused by deep structures are of lower amplitude and greater extent than those caused by shallow sources. This wavenumber–amplitude relationship to depth may be quantified to compute the maximum depth (or limiting depth) at which the top of the anomalous body could be situated.

(a) Half-width method. The half-width of an anomaly ($x_{1/2}$) is the horizontal distance from the anomaly maximum to the point at which the anomaly has reduced to half of its maximum value (Fig. 6.18(a)).

If the anomaly is three-dimensional, the initial assumption is made that it results from a point mass. Manipulation of the point mass formula (equation (6.6)) allows its depth to be determined in terms of the half-width

$$z = \frac{x_{1/2}}{\sqrt{\sqrt[3]{4} - 1}}$$

Here, z represents the actual depth of the point mass or the centre of a sphere with the same mass. It is an overestimate of the depth to the top of the sphere, that is, the limiting depth. Consequently, the limiting depth for any three-dimensional body is given by

$$z < \frac{x_{1/2}}{\sqrt{\sqrt[3]{4} - 1}} \tag{6.15}$$

A similar approach is adopted for a two-dimensional anomaly, with the initial assumption that the anomaly

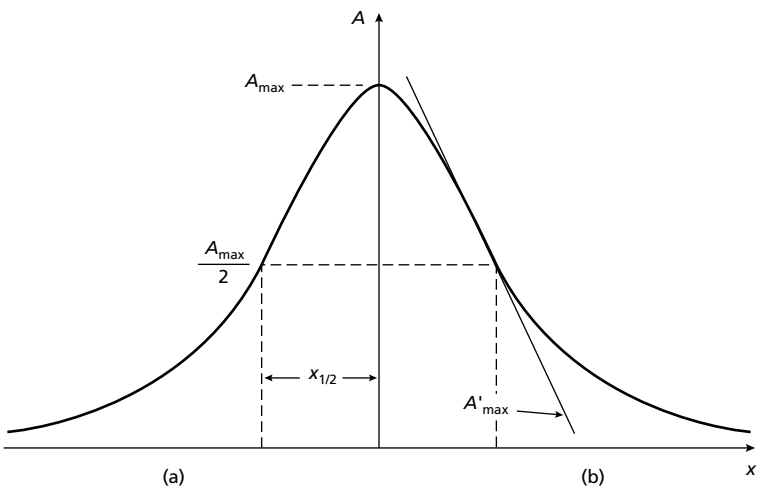

Fig. 6.18 Limiting depth calculations using (a) the half-width method and (b) the gradient–amplitude ratio.

results from a horizontal line mass (equation (6.7)). The depth to a line mass or to the centre of a horizontal cylinder with the same mass distribution is given by

$$z = x_{1/2}$$

For any two-dimensional body, the limiting depth is then given by

$$z < x_{1/2} \tag{6.16}$$

(b) Gradient–amplitude ratio method. This method requires the computation of the maximum anomaly amplitude (A_{max}) and the maximum horizontal gravity gradient (A'_{max}) (Fig. 6.18(b)). Again the initial assumption is made that a three-dimensional anomaly is caused by a point mass and a two-dimensional anomaly by a line mass. By differentiation of the relevant formulae, for any three-dimensional body

$$z < 0.86 \left| \frac{A_{max}}{A'_{max}} \right| \tag{6.17}$$

and for any two-dimensional body

$$z < 0.65 \left| \frac{A_{max}}{A'_{max}} \right| \tag{6.18}$$

(c) Second derivative methods. There are a number of limiting depth methods based on the computation of the maximum second horizontal derivative, or maximum rate of change of gradient, of a gravity anomaly (Smith 1959). Such methods provide rather more accurate limiting depth estimates than either the half-width or gradient–amplitude ratio methods if the observed anomaly is free from noise.

Excess mass

The excess mass of a body can be uniquely determined from its gravity anomaly without making any assumptions about its shape, depth or density. Excess mass refers to the difference in mass between the body and the mass of country rock that would otherwise fill the space occupied by the body. The basis of this calculation is a formula derived from Gauss' theorem, and it involves a surface integration of the residual anomaly over the area in which it occurs. The survey area is divided into n grid squares of area Δa and the mean residual anomaly Δg found for each square. The excess mass M_e is then given by

$$M_e = \frac{1}{2\pi G} \sum_{i=1}^{n} \Delta g_i \Delta a_i \tag{6.19}$$

Before using this procedure it is important that the regional field is removed so that the anomaly tails to zero. The method only works well for isolated anomalies whose extremities are well defined. Gravity anomalies decay slowly with distance from source and so these tails can cover a wide area and be important contributors to the summation.

To compute the actual mass M of the body, the densities of both anomalous body (ρ_1) and country rock (ρ_2) must be known:

$$M = \frac{\rho_1 M_e}{(\rho_1 - \rho_2)} \tag{6.20}$$

The method is of use in estimating the tonnage of ore bodies. It has also been used, for example, in the estimation of the mass deficiency associated with the Chicxulub crater, Yucatan (CamposEnriquez *et al.* 1998), whose formation due to meteorite or asteroid impact has been associated with the extinction of the dinosaurs.

Inflection point

The locations of inflection points on gravity profiles, i.e. positions where the horizontal gravity gradient changes most rapidly, can provide useful information on the nature of the edge of an anomalous body. Over structures with outward dipping contacts, such as granite bodies (Fig. 6.19(a)), the inflection points (arrowed) lie near the base of the anomaly. Over structures with inward dipping contacts such as sedimentary basins (Fig. 6.19(b)), the inflection points lie near the uppermost edge of the anomaly.

Approximate thickness

If the density contrast $\Delta\rho$ of an anomalous body is known, its thickness t may be crudely estimated from its maximum gravity anomaly Δg by making use of the Bouguer slab formula (equation (6.8)):

$$t \approx \frac{\Delta g}{2\pi G \Delta\rho} \tag{6.21}$$

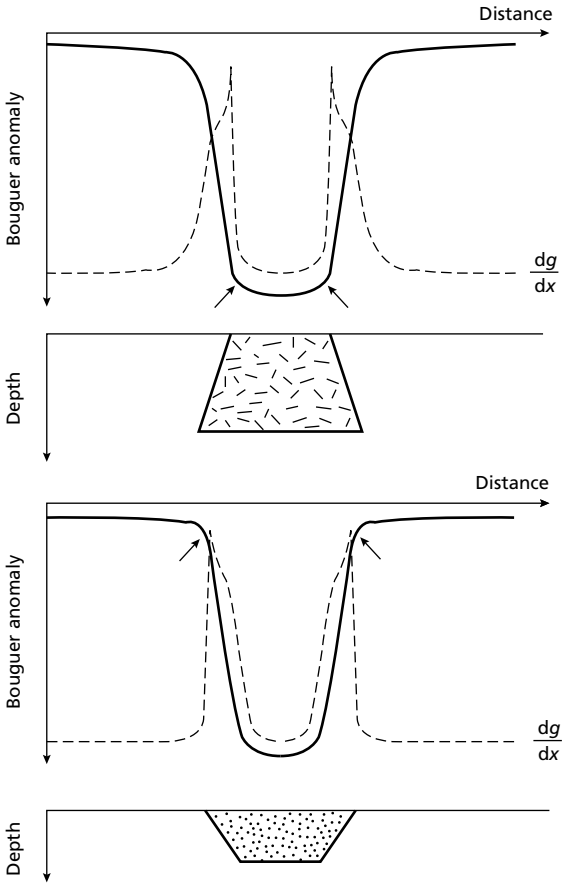

Fig. 6.19 Bouguer anomaly profiles across (a) a granite body, and (b) a sedimentary basin. The inflection points are marked with an arrow. The broken lines represent the horizontal derivative (rate of change of gradient) of the gravity anomaly, which is at a maximum at the inflection points.

This thickness will always be an underestimate for a body of restricted horizontal extent. The method is commonly used in estimating the throw of a fault from the difference in the gravity fields of the upthrown and downthrown sides.

The technique of source depth determination by Euler deconvolution, described in Section 7.10.2, is also applicable to gravity anomalies (Keating 1998).

6.10.4 Indirect interpretation

In indirect interpretation, the causative body of a gravity anomaly is simulated by a model whose theoretical anomaly can be computed, and the shape of the model is altered until the computed anomaly closely matches the observed anomaly. Because of the inverse problem this model will not be a unique interpretation, but ambiguity can be decreased by using other constraints on the nature and form of the anomalous body.

A simple approach to indirect interpretation is the comparison of the observed anomaly with the anomaly computed for certain standard geometrical shapes whose size, position, form and density contrast are altered to improve the fit. Two-dimensional anomalies may be compared with anomalies computed for horizontal cylinders or half-cylinders, and three-dimensional anomalies compared with those of spheres, vertical cylinders or right rectangular prisms. Combinations of such shapes may also be used to simulate an observed anomaly.

Figure 6.20(a) shows a large, circular gravity anomaly situated near Darnley Bay, NWT, Canada. The anomaly is radially symmetrical and a profile across the anomaly (Fig. 6.20(b)) can be simulated by a model constructed from a suite of coaxial cylinders whose diameters decrease with depth so that the anomalous body has the overall form of an inverted cone. This study illustrates well the non-uniqueness of gravity interpretation. The nature of the causative body is unknown and so no information is available on its density. An alternative interpretation, again in the form of an inverted cone, but with an increased density contrast, is presented in Fig. 6.20(b). Both models provide adequate simulations of the observed anomaly, and cannot be distinguished using the information available.

The computation of anomalies over a model of irregular form is accomplished by dividing the model into a series of regularly-shaped compartments and calculating the combined effect of these compartments at each observation point. At one time this operation was performed by the use of graticules, but nowadays the calculations are invariably performed by computers.

A two-dimensional gravity anomaly may be represented by a profile normal to the direction of elongation. This profile can be interpreted in terms of a model which maintains a constant cross-section to infinity in the horizontal directions perpendicular to the profile.

The basic unit for constructing the anomaly of a two-dimensional model is the semi-infinite slab with a sloping edge shown in Fig. 6.21, which extends to infinity into and out of the plane of the figure. The gravity anomaly of this slab Δg is given by

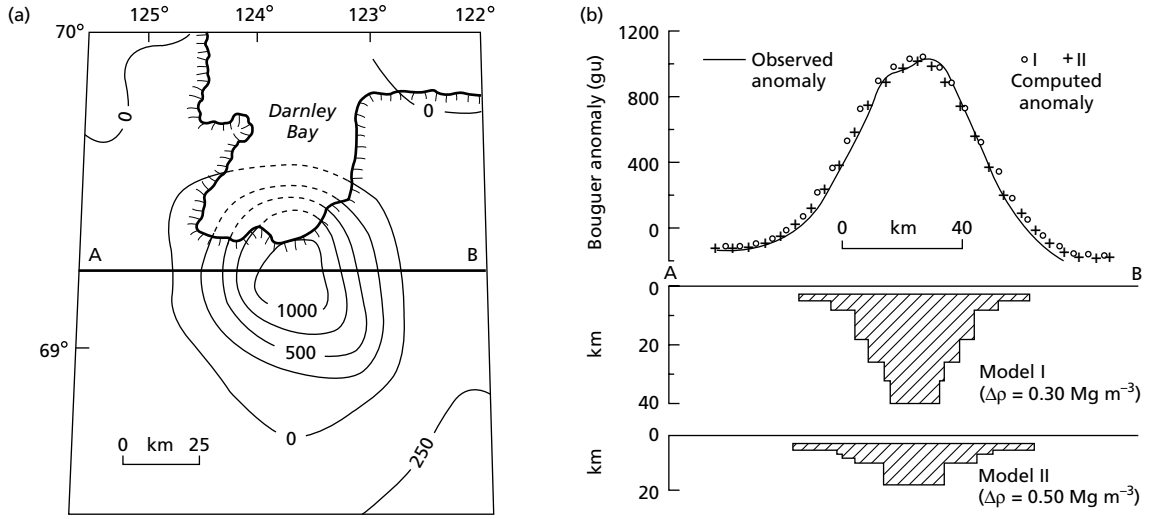

Fig. 6.20 (a) The circular gravity anomaly at Darnley Bay, NWT, Canada. Contour interval 250 gu. (b) Two possible interpretations of the anomaly in terms of a model constructed from a suite of coaxial vertical cylinders. (After Stacey 1971.)

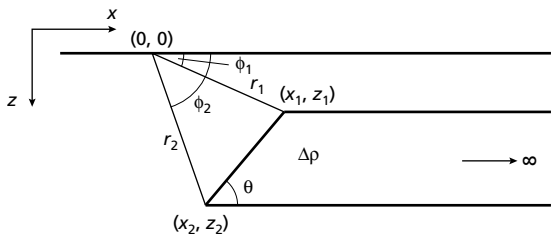

Fig. 6.21 Parameters used in defining the gravity anomaly of a semi-infinite slab with a sloping edge.

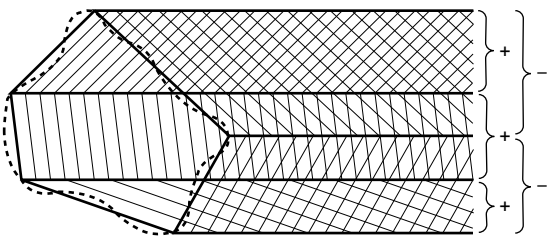

Fig. 6.22 The computation of gravity anomalies of two-dimensional bodies of irregular cross-section. The body (dashed line) is approximated by a polygon and the effects of semi-infinite slabs with sloping edges defined by the sides of the polygon are progressively added and subtracted until the anomaly of the polygon is obtained.

$$\Delta g = 2G\Delta\rho[-\{x_1 \sin\theta + z_1 \cos\theta\} \times \{\sin\theta \log_e(r_2/r_1) + \cos\theta(\phi_2 - \phi_1)\} + z_2\phi_2 - z_1\phi_1] \quad (6.22)$$

where $\Delta\rho$ is the density contrast of the slab, angles are expressed in radians and other parameters are defined as in Fig. 6.21 (Talwani *et al.* 1959). To calculate the anomaly of a two-dimensional body of irregular cross-section, the body is approximated by a polygon as shown in Fig. 6.22. The anomaly of the polygon is then found by proceeding around it summing the anomalies of the slabs bounded by edges where the depth increases and subtracting those where the depth decreases.

Figure 6.23 illustrates a two-dimensional interpretation, in terms of a model of irregular geometry represented by a polygonal outline, of the Bodmin Moor granite of southwest England. The shape of the uppermost part of the model is controlled by the surface outcrop of granite, while the density contrasts employed are based on density measurements on rock samples. The interpretation shows unambiguously that the contacts of the granite slope outwards. Ambiguity is evident, however, in the interpretation of the gravity gradient over the northern flank of the granite. The model presented in Fig. 6.23 interprets the cause of this gradient as a

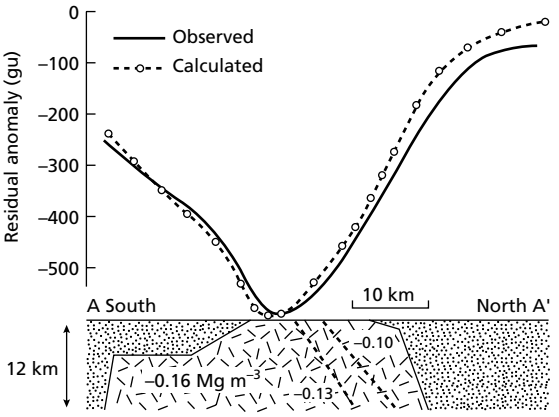

Fig. 6.23 A two-dimensional interpretation of the gravity anomaly of the Bodmin Moor granite, southwest England. See Fig. 6.27 for location. (After Bott & Scott 1964.)

northerly increase in the density of the granite; a possible alternative, however, would be a northerly thinning of a granite body of constant density contrast.

Two-dimensional methods can sometimes be extended to three-dimensional bodies by applying end-correction factors to account for the restricted extent of the causative body in the strike direction (Cady 1980). The end-correction factors are, however, only approximations and full three-dimensional modelling is preferable.

The gravity anomaly of a three-dimensional body may be calculated by dividing the body into a series of horizontal slices and approximating each slice by a polygon (Talwani & Ewing 1960). Alternatively the body may be constructed out of a suite of right rectangular prisms.

However a model calculation is performed, indirect interpretation involves four steps:

1. Construction of a reasonable model.
2. Computation of its gravity anomaly.
3. Comparison of computed with observed anomaly.
4. Alteration of model to improve correspondence of observed and calculated anomalies and return to step 2.

The process is thus iterative and the goodness of fit between observed and calculated anomalies is gradually improved. Step 4 can be performed manually for bodies of relatively simple geometry so that an interpretation is readily accomplished using interactive routines on a personal computer (Götze & Lahmeyer 1988). Bodies of complex geometry in two- or three-dimensions are not so simply dealt with and in such cases it is advantageous to employ techniques which perform the iteration automatically.

The most flexible of such methods is *non-linear optimization* (Al-Chalabi 1972). All variables (body points, density contrasts, regional field) may be allowed to vary within defined limits. The method then attempts to minimize some function F which defines the goodness of fit, for example

$$F = \sum_{i=1}^{n} \left(\Delta g_{\text{obs}_i} - \Delta g_{\text{calc}_i}\right)^2$$

where Δg_{obs} and Δg_{calc} are series of n observed and calculated values.

The minimization proceeds by altering the values of the variables within their stated limits to produce a successively smaller value for F for each iteration. The technique is elegant and successful but expensive in computer time.

Other such automatic techniques involve the simulation of the observed profile by a thin layer of variable density. This *equivalent layer* is then progressively expanded so that the whole body is of a uniform, specified density contrast. The body then has the form of a series of vertical prisms in either two or three dimensions which extend either above, below or symmetrically around the original equivalent layer. Such methods are less flexible than the non-linear optimization technique in that usually only a single density contrast may be specified and the model produced must either have a specified base or top or be symmetrical about a central horizontal plane.

6.11 Elementary potential theory and potential field manipulation

Gravitational and magnetic fields are both potential fields. In general the potential at any point is defined as the work necessary to move a unit mass or pole from an infinite distance to that point through the ambient field. Potential fields obey Laplace's equation which states that the sum of the rates of change of the field gradient in three orthogonal directions is zero. In a normal Cartesian coordinate system with horizontal axes x, y and a vertical axis z, Laplace's equation is stated

$$\frac{\partial^2 A}{\partial x^2} + \frac{\partial^2 A}{\partial y^2} + \frac{\partial^2 A}{\partial z^2} = 0 \qquad (6.23)$$

where A refers to a gravitational or magnetic field and is a function of (x, y, z).

In the case of a two-dimensional field there is no variation along one of the horizontal directions so that A is a function of x and z only and equation (6.23) simplifies to

$$\frac{\partial^2 A}{\partial x^2} + \frac{\partial^2 A}{\partial z^2} = 0 \tag{6.24}$$

Solution of this partial differential equation is easily performed by separation of variables

$$A_k(x, z) = (a \cos kx + b \sin kx)\, e^{kz} \tag{6.25}$$

where a and b are constants, the positive variable k is the spatial frequency or wavenumber, A_k is the potential field amplitude corresponding to that wavenumber and z is the level of observation. Equation (6.25) shows that a potential field can be represented in terms of sine and cosine waves whose amplitude is controlled exponentially by the level of observation.

Consider the simplest possible case where the two-dimensional anomaly measured at the surface $A(x, 0)$ is a sine wave

$$A(x, 0) = A_0 \sin kx \tag{6.26}$$

where A_0 is a constant and k the wavenumber of the sine wave. Equation (6.25) enables the general form of the equation to be stated for any value of z

$$A(x, z) = (A_0 \sin kx)\, e^{kz} \tag{6.27}$$

The field at a height h above the surface can then be determined by substitution in equation (6.27)

$$A(x, -h) = (A_0 \sin kx)\, e^{-kh} \tag{6.28}$$

and the field at depth d below the surface

$$A(x, d) = (A_0 \sin kx)\, e^{kd} \tag{6.29}$$

The sign of h and d is important as the z-axis is normally defined as positive downwards.

Equation (6.27) is an over-simplification in that a potential field is never a function of a single sine wave. Invariably such a field is composed of a range of wavenumbers. However, the technique is still valid as long as the field can be expressed in terms of all its component wavenumbers, a task easily performed by use of the Fourier transform (Section 2.3). If, then, instead of the terms $(a \cos kx + b \sin kx)$ in equation (6.25) or $(A_0 \sin kx)$ in equation (6.27), the full Fourier spectrum, derived by Fourier transformation of the field into the wavenumber domain, is substituted, the results of equations (6.28) and (6.29) remain valid.

These latter equations show that the field measured at the surface can be used to predict the field at any level above or below the plane of observation. This is the basis of the upward and downward field continuation methods in which the potential field above or below the original plane of measurement is calculated in order to accentuate the effects of deep or shallow structures respectively.

Upward continuation methods are employed in gravity interpretation to determine the form of regional gravity variation over a survey area, since the regional field is assumed to originate from relatively deep-seated structures. Figure 6.24(a) is a Bouguer anomaly map of the Saguenay area in Quebec, Canada, and Fig. 6.24(b) represents the field continued upward to an elevation of 16 km. Comparison of the two figures clearly illustrates how the high-wavenumber components of the observed field have been effectively removed by the continuation process. The upward continued field must result from relatively deep structures and consequently represents a valid regional field for the area. Upward continuation is also useful in the interpretation of magnetic anomaly fields (see Chapter 7) over areas containing many near-surface magnetic sources such as dykes and other intrusions. Upward continuation attenuates the high-wavenumber anomalies associated with such features and enhances, relatively, the anomalies of the deeper-seated sources.

Downward continuation of potential fields is of more restricted application. The technique may be used in the resolution of the separate anomalies caused by adjacent structures whose effects overlap at the level of observation. On downward continuation, high-wavenumber components are relatively enhanced and the anomalies show extreme fluctuations if the field is continued to a depth greater than that of its causative structure. The level at which these fluctuations commence provides an estimate of the limiting depth of the anomalous body. The effectiveness of this method is diminished if the potential field is contaminated with noise, as the noise is accentuated on downward continuation.

The selective enhancement of the low- or high-wavenumber components of potential fields may be achieved in a different but analogous manner by the

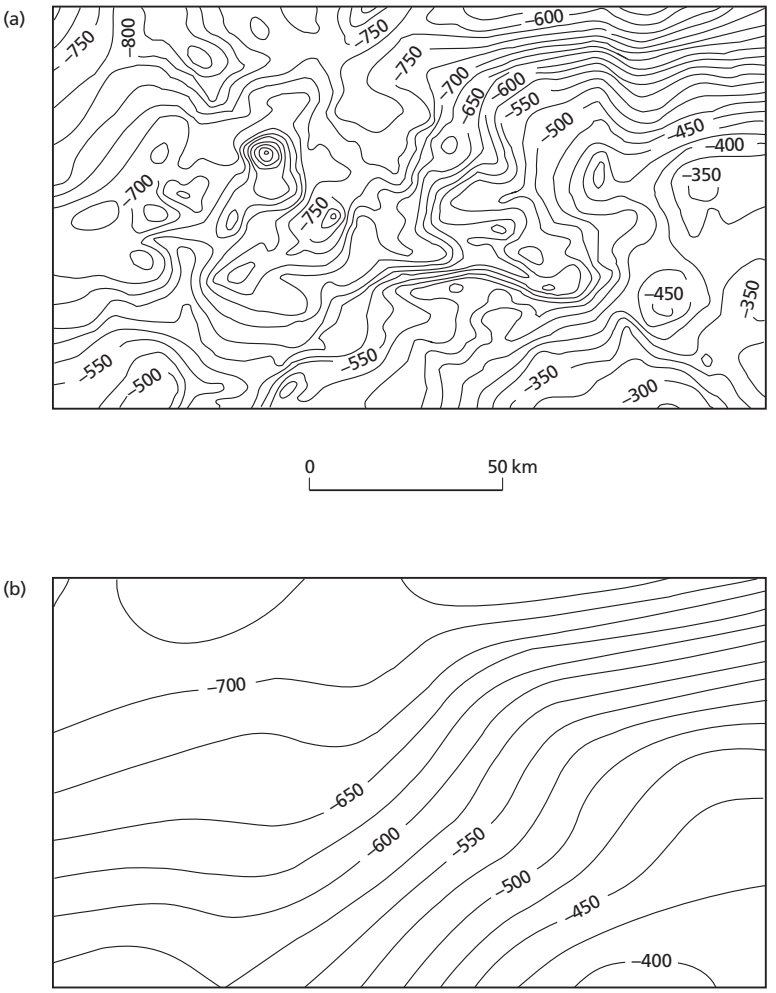

Fig. 6.24 (a) Observed Bouguer anomalies (gu) over the Saguenay area, Quebec, Canada. (b) The gravity field continued upward to an elevation of 16 km. (After Duncan & Garland 1977.)

application of *wavenumber filters*. Gravitational and magnetic fields may be processed and analysed in a similar fashion to seismic data, replacing frequency by wavenumber. Such processing is more complex than the equivalent seismic filtering as potential field data are generally arranged in two horizontal dimensions, that is, contour maps, rather than a single dimension. However, it is possible to devise two-dimensional filters for the selective removal of high- or low-wavenumber components from the observed anomalies. The consequence of the application of such techniques is similar to upward or downward continuation in that shallow structures are mainly responsible for the high-wavenumber components of anomalies and deep structures for the low wavenumbers. However, it is not possible fully to isolate local or regional anomalies by wavenumber filtering because the wavenumber spectra of deep and shallow sources overlap.

Other manipulations of potential fields may be accomplished by the use of more complex filter operators (e.g. Gunn 1975, Cooper 1997). Vertical or horizontal derivatives of any order may be computed from the observed field. Such computations are not widely employed, but second horizontal derivative maps are occasionally used for interpretation as they accentuate anomalies associated with shallow bodies.

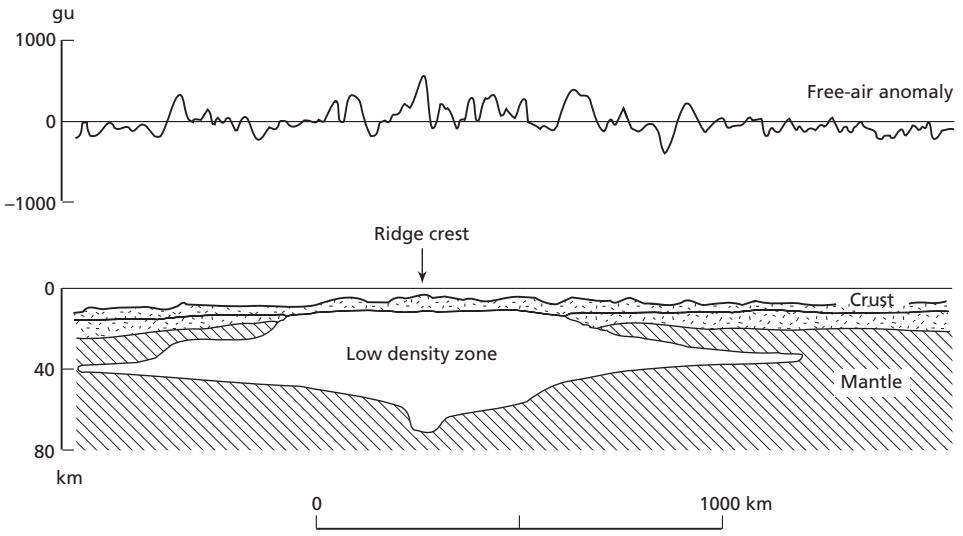

Fig. 6.25 Free-air anomaly profile across the mid-Atlantic ridge. (After Talwani *et al.* 1965.)

6.12 Applications of gravity surveying

Gravity studies are used extensively in the investigation of large- and medium-scale geological structures (Paterson & Reeves 1985). Early marine surveys, performed from submarines, indicated the existence of large positive and negative gravity anomalies associated with island arcs and oceanic trenches, respectively; subsequent shipborne work has demonstrated their lateral continuity and has shown that most of the major features of the Earth's surface can be delineated by gravity surveying. Gravity anomalies have also shown that most of these major relief features are in isostatic equilibrium, suggesting that the lithosphere is not capable of sustaining significant loads and yields isostatically to any change in surface loading. Figure 6.25 shows the near-zero free-air anomalies over an ocean ridge which suggest that it is in isostatic equilibrium. The gravity interpretation, which is constrained by seismic refraction results, indicates that this compensation takes the form of a zone of mass deficiency in the underlying mantle. Its low seismic velocity and the high heat flow at the surface suggest that this is a region of partial melting and, perhaps, hydration. Gravity surveying can also be used in the study of ancient suture zones, which are interpreted as the sites of former plate boundaries within the continental lithosphere. These zones are often characterized by major linear gravity anomalies resulting from the different crustal sections juxtaposed across the sutures (Fig. 6.26).

On the medium scale, gravity anomalies can reveal the subsurface form of igneous intrusions such as granite batholiths and anorthosite massifs. For example, gravity surveys in southwest England (Bott *et al.* 1958) have revealed a belt of large-amplitude, negative Bouguer anomalies overlying a region of outcropping granites (Fig. 6.27). Modelling of the gravity anomalies (Fig. 6.23) has led to the postulation of a continuous batholith some 10–15 km thick underlying southwest England (see e.g. Brooks *et al.* 1983). Studies such as these have provided important constraints on the mechanism of emplacement, composition and origin of igneous bodies. Similarly, gravity surveying has been extensively used in the location of sedimentary basins, and their interpreted structures have provided important information on mechanisms of basin formation.

The gravity method was once extensively used by the petroleum industry for the location of possible hydrocarbon traps, but the subsequent vast improvement in efficiency and technology of seismic surveying has led to the demise of gravity surveying as a primary exploration tool.

In commercial applications, gravity surveying is rarely used in reconnaissance exploration. This is because the method is relatively slow to execute, and therefore expensive, due to the necessity of accurately determined elevations and the length of the reduction procedure. Gravity methods do find application, however, as a follow-up technique used on a target defined by

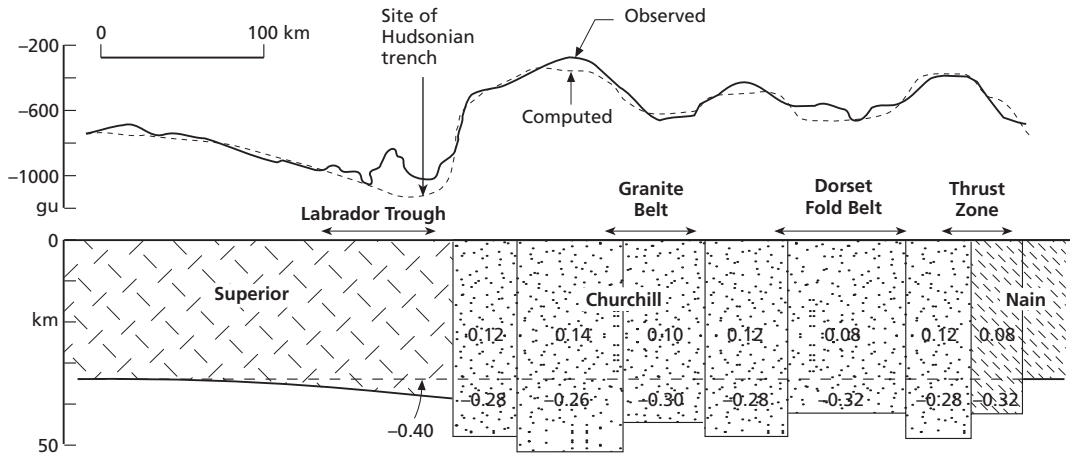

Fig. 6.26 Bouguer anomaly profile across a structural province boundary in the Canadian Shield. Density contrasts in Mg m^{-3}. (After Thomas & Kearey 1980.)

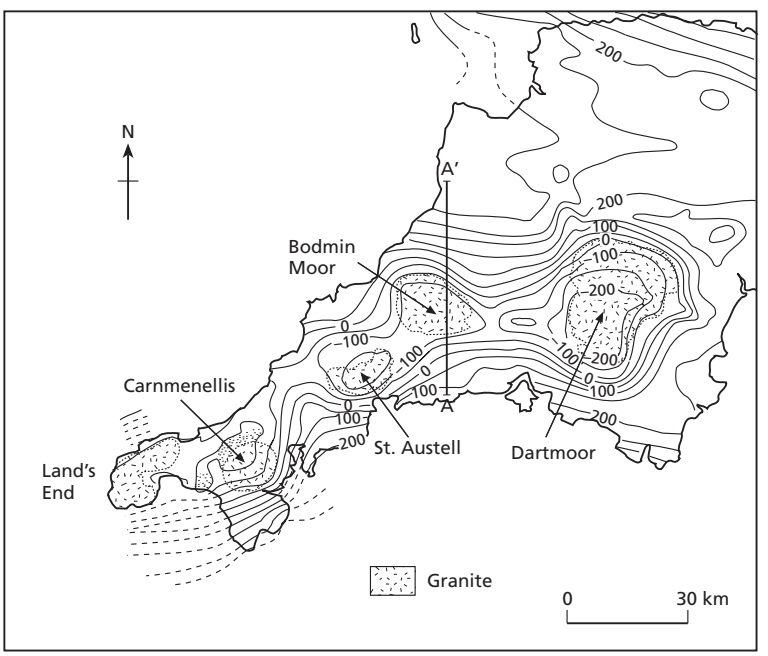

Fig. 6.27 Bouguer anomaly map of southwest England, showing a linear belt of large negative anomalies associated with the zone of granite outcrops. Contour interval 50 gu. (After Bott & Scott 1964.)

another, more cost-effective method. An important application of this type in mineral exploration is the determination of ore tonnage by the excess mass method described in Section 6.10.3.

Gravity surveying may be used in hydrogeological investigations to determine the geometry of potential aquifers. Figure 6.28 shows a Bouguer anomaly map of an area near Taltal, Chile (Van Overmeeren 1975). The region is extremely arid, with groundwater supply and storage controlled by deep geological features. The gravity minima revealed by the contours probably represent two buried valleys in the alluvium overlying the granodioritic bedrock. Figure 6.29 shows an interpretation of a profile over the minima. The bedrock topography was controlled by the results from a seismic refraction line which had been interpreted using the plus–minus

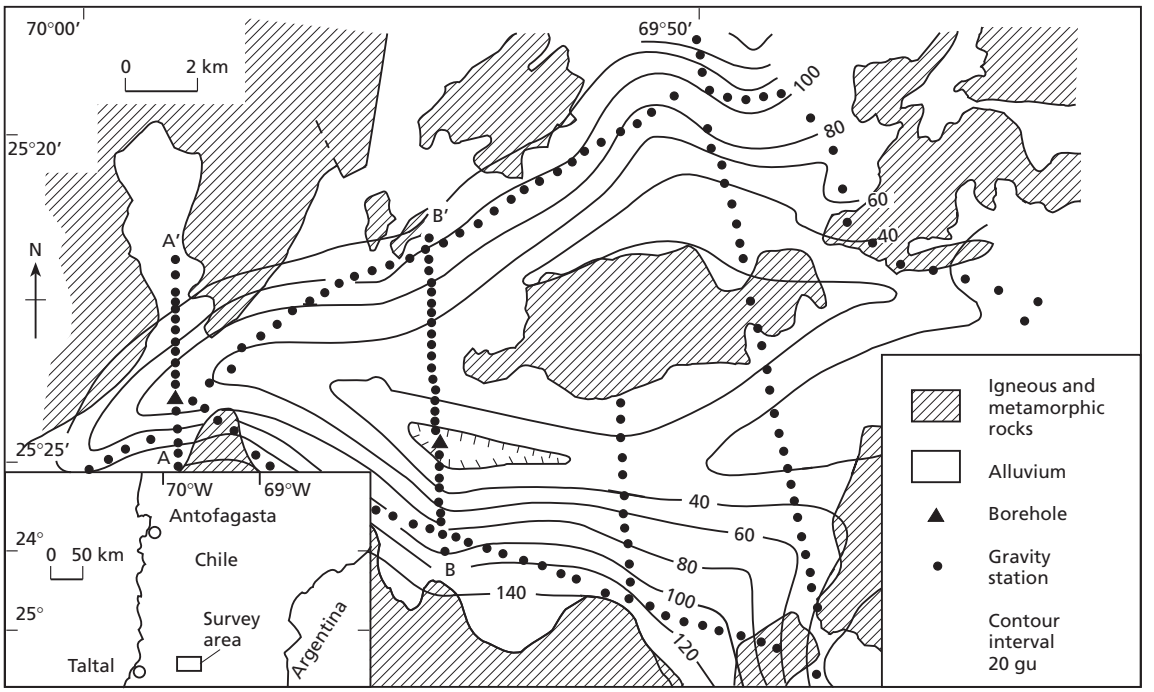

Fig. 6.28 Geological map of an area near Taltal, Chile, showing location of gravity stations and contoured Bouguer anomalies. (After Van Overmeeren 1975.)

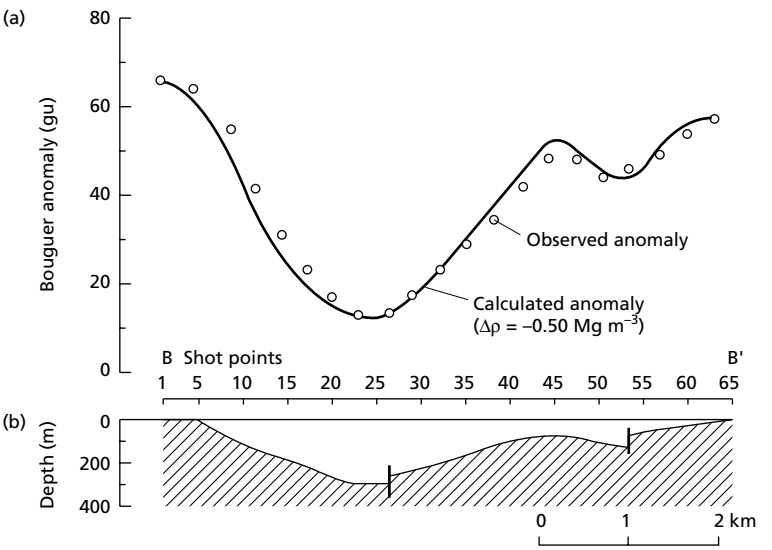

Fig. 6.29 Profile B–B′, Taltal area, Chile (see Fig. 6.28 for location). (a) Observed Bouguer anomaly and calculated anomaly for a model with a density contrast ($\Delta\rho$) of $-0.50\ \mathrm{Mg\,m^{-3}}$. (b) Gravity interpretation. (After Van Overmeeren 1975.)

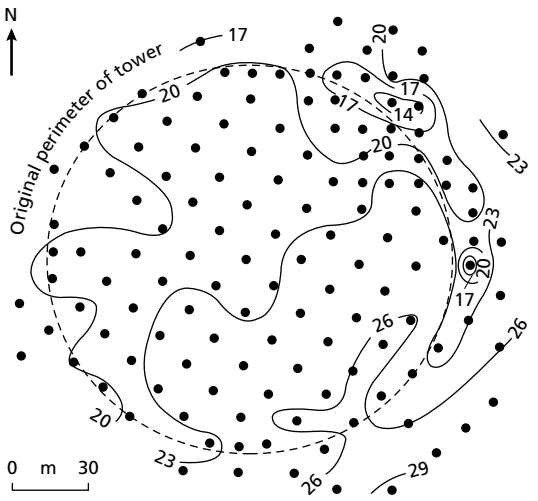

Fig. 6.30 Bouguer anomalies, uncorrected for topographic effects, over the cooling tower area. Contour interval 0.3 gu. (After Arzi 1975.)

method (see Section 5.4). The seismic control allowed a mean density of the highly variable valley-fill deposits to be determined. On the basis of the geophysical results, two boreholes (Fig. 6.28) were sunk in the deepest parts of the valley fill and located groundwater ponded in the bedrock depressions.

In engineering and geotechnical applications, gravity surveying is sometimes used in the location of subsurface voids. Void detection has been made possible by the development of microgravimetric techniques which can detect gravity changes as small as a microgal. Arzi (1975) described a microgravity survey of the proposed site of a cooling tower serving a nuclear power plant, where it was suspected that solution cavities might be present in the dolomitic bedrock. Measurements were made on a 15 m grid at points whose elevations had been determined to ±3 mm, with base readings at 40 min intervals. The soil thickness had been determined so that its effects could be computed and 'stripped' from the observations to remove gravity variations caused by undulating bedrock topography. The resulting Bouguer anomaly map is shown in Fig. 6.30. In the NE part of the site there are two minima near the proposed perimeter of the cooling tower, and subsequent drilling confirmed that they originated from buried cavities. Remedial work entailed the injection of grouting material into the cavities. A check on the effectiveness of the grouting was provided by a repeat gravity survey which, by an excess mass calculation (Section 6.10.3), showed that the change in the gravity field before and after grouting was caused by the replacement of voids by grouting material. Casten and Gram (1989) have described microgravity surveys performed underground to locate cavities which might pose a threat to the safety of mine workings.

Microgravity surveys also find application in archaeological investigations, where they may be used in the detection of buried buildings, tombs and other artefacts. The technique has also been used to study the temporal movement of groundwater through a region.

An important recent development in gravity surveying is the design of portable instruments capable of measuring absolute gravity with high precision. Although the cost of such instruments is high it is possible that they will be used in the future to investigate large-scale mass movements in the Earth's interior and small cyclic gravity variations associated with neotectonic phenomena such as earthquakes and postglacial uplift.

Gravitational studies, both of the type described in this chapter and satellite observations, are important in geodesy, the study of the shape of the Earth. Gravity surveying also has military significance, since the trajectory of a missile is affected by gravity variation along its flight path.

Problems

1. Compare and contrast the LaCoste–Romberg and Worden-type gravimeters. State also the advantages and disadvantages of the two types of instrument.

2. What are the magnitudes of the terrain correction at gravity stations (a) at the top, (b) at the base, and (c) half-way up a vertical cliff 100 m high?

3. The table shows data collected along a north–south gravity profile. Distances are measured from the south end of the profile, whose latitude is 51°12′24″N. The calibration constant

of the Worden gravimeter used on the survey is 3.792 gu per dial unit. Before, during and after the survey, readings (marked BS) were taken at a base station where the value of gravity is 9 811 442.2 gu. This was done in order to monitor instrumental drift and to allow the absolute value of gravity to be determined at each observation point.

Station	Time	Dist. (m)	Elev. (m)	Reading
BS	0805			2934.2
1	0835	0	84.26	2946.3
2	0844	20	86.85	2941.0
3	0855	40	89.43	2935.7
4	0903	60	93.08	2930.4
1	0918			2946.5
BS	0940			2934.7
1	1009			2946.3
5	1024	80	100.37	2926.6
6	1033	100	100.91	2927.9
7	1044	120	103.22	2920.0
X	1053	140	107.35	2915.1
1	1111			2946.5
BS	1145			2935.2
1	1214			2946.2
9	1232	160	110.10	2911.5
10	1242	180	114.89	2907.2
11	1300	200	118.96	2904.0
1	1315			2946.3
BS	1350			2935.5

(a) Perform a gravity reduction of the survey data and comment on the accuracy of each step. Use a density of 2.70 $Mg\,m^{-3}$ for the Bouguer correction.
(b) Draw a series of sections illustrating the variation in topography, observed gravity, free-air anomaly and Bouguer anomaly along the profile. Comment on the sections.
(c) What further information would be required before a full interpretation could be made of the Bouguer anomaly?

4. Two survey vessels with shipborne gravity meters are steaming at 6 knots in opposite directions along an east–west course. If the difference in gravity read by the two meters is 635 gu as the ships pass, what is the latitude?

5. The gravity anomaly Δg of an infinite horizontal slab of thickness t and density contrast $\Delta\rho$ is given by

$$\Delta g = 2\pi G \Delta\rho t$$

where the gravitational constant G is $6.67 \times 10^{-11}\,m^3\,kg^{-1}\,s^{-2}$.
(a) Scale this equation to provide Δg in gu when $\Delta\rho$ is expressed in $Mg\,m^{-3}$ and t in m.
(b) This equation is used to provide a preliminary estimate of the gravity anomaly of a body of specified thickness. Using this equation, calculate the gravity anomaly of (i) a granite 12 km thick of density 2.67 $Mg\,m^{-3}$; and (ii) a sandstone body 4 km thick of density 2.30 $Mg\,m^{-3}$, where the density of the surrounding metamorphic rocks is 2.80 $Mg\,m^{-3}$. Are the anomalies so calculated liable to be over- or underestimates?

6. Show that the half-width of the gravity anomaly caused by a horizontal cylinder is equal to the depth of the axis of the cylinder.

7. Figure 6.31 is a Bouguer anomaly map, contoured at an interval of 50 gu, of a drift-covered area.
(a) On the map, sketch in what you consider to be the regional field and then remove it from the observed field to isolate residual anomalies,

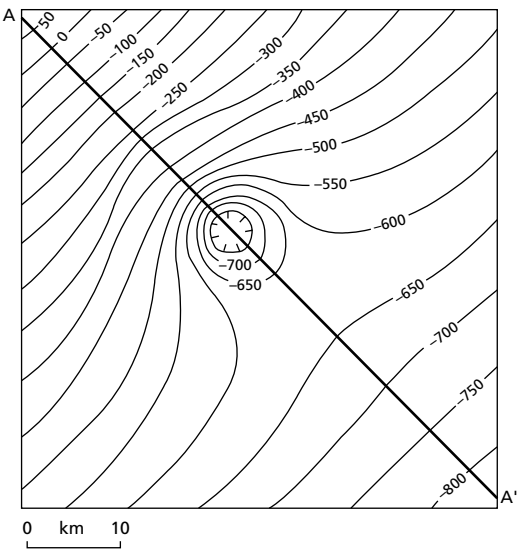

Fig. 6.31 Bouguer anomaly map pertaining to Question 7. Contour interval 50 gu.

Continued

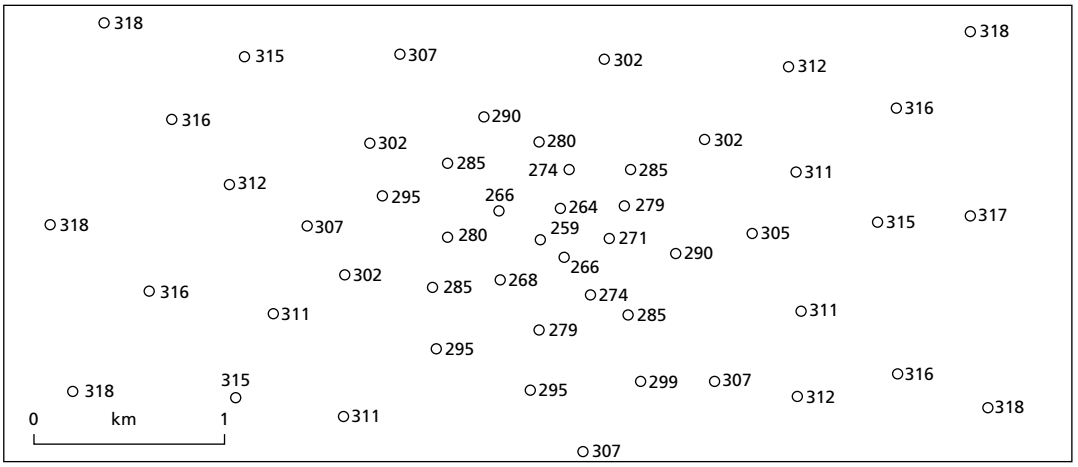

Fig. 6.32 Bouguer anomaly observations pertaining to Question 8. Values in gu.

which can be represented on the map as contours drawn in a different colour.

(b) Construct gravity profiles along line A–A′ illustrating the observed, regional and residual anomalies.

(c) Perform a direct interpretation of the residual anomaly, obtaining as much information as possible on the depth, thickness and shape of the source.

(d) The bedrock constitutes part of a Precambrian shield. Speculate on the nature of the anomalous body, giving reasons for your ideas.

8. Contour the gravity data on the map shown in Fig. 6.32 using an interval of 10 gu. Draw a representative profile.

(a) Use limiting depth calculations based on the half-width and gradient–amplitude methods to determine the depth to the centre of mass of the anomalous body. Comment on any difference between the depth estimates provided by the two methods.

(b) Determine the mass deficiency present using the formula for the gravity anomaly of a point mass. If the anomaly is caused by a salt dome of density 2.22 $Mg\,m^{-3}$ within sediments of density 2.60 $Mg\,m^{-3}$, calculate the volume and mass of salt present and the depth to the top of the salt dome. Compute the actual gravity anomaly of the salt and comment on any differences with the observed anomaly.

(c) What is the lowest possible density contrast of the anomalous body?

(d) Determine the mass deficiency present using a method based on Gauss' Theorem. Comment on the accuracy of the value obtained and compare it with the answer to (b). Calculate the actual mass present assuming the same densities as in (a).

9. The map in Fig. 6.33 shows Bouguer anomalies over a gabbro intrusion in a schist terrain. In the eastern part of the map, horizontally bedded Mesozoic sediments unconformably overlie the schists. A seismic refraction line has been established over the sediments in the location shown. Time–distance data and typical velocities and densities are given below.

Interpret the geophysical results using the following scheme:

(a) Use the refraction data to determine the thickness and possible nature of the Mesozoic rocks beneath the seismic line.

(b) Use this interpretation to calculate the gravity anomaly of the Mesozoic rocks at this location. Correct the observed gravity anomaly for the effect of the Mesozoic rocks.

(c) Determine the maximum gravity anomaly of

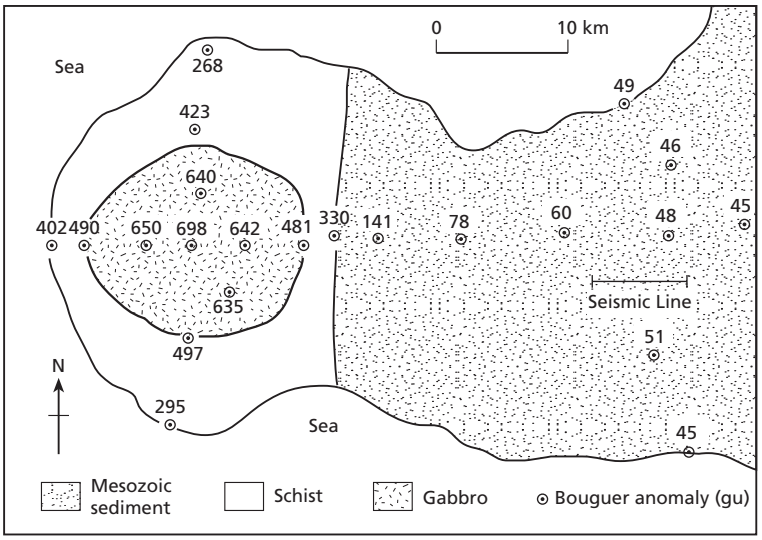

Fig. 6.33 Map of geophysical observations pertaining to Question 9. Bouguer anomaly values in gu.

the gabbro. Assuming the gabbro to have the form of a vertical cylinder, determine the depth to its base.

The gravity anomaly Δg of a vertical cylinder of density contrast $\Delta\rho$, radius r, length L, depth to top z_U and depth to base z_L is given by

$$\Delta g = 2\pi G\Delta\rho\left(L - \sqrt{z_L^2 + r^2} + \sqrt{z_U^2 + r^2}\right)$$

where G is the gravitational constant.

State any assumptions and possible causes of error in your interpretation.

Typical densities and seismic velocities

	ρ (Mg m^{-3})	Veloc. (km s^{-1})
Jur./Cret.	2.15	1.20–1.80
Trias	2.35	2.40–3.00
Schist	2.75	3.60–4.90
Gabbro	2.95	

Jur. = Jurassic; Cret. = Cretaceous.

Seismic data

Dist. (m)	Time (s)
530	0.349
600	0.391
670	0.441
1130	0.739
1200	0.787
1270	0.831
1800	1.160
1870	1.177
1940	1.192
2730	1.377
2800	1.393
2870	1.409
3530	1.563
3600	1.582
3670	1.599

10. Over a typical ocean spreading centre, the free-air gravity anomaly is approximately zero and the Bouguer anomaly is large and negative. Why?

Further reading

Baranov, W. (1975) *Potential Fields and Their Transformations in Applied Geophysics*. Gebrüder Borntraeger, Berlin.

Blakely, R.J. (1995) *Potential Theory in Gravity and Magnetic Applications*. Cambridge University Press, Cambridge.

Bott, M.H.P. (1973) Inverse methods in the interpretation of magnetic and gravity anomalies. In: Alder, B., Fernbach, S. & Bolt, B.A. (eds), *Methods in Computational Physics*, **13**, 133–62.

Dehlinger, P. (1978) *Marine Gravity*. Elsevier, Amsterdam.

Gibson, R.I. & Millegan, P.S. (eds) (1998) *Geologic Applications of*

Gravity and Magnetics: Case Histories. SEG Reference Series 8 & AAPG Studies in Geology 43, Tulsa.

LaCoste, L.J.B. (1967) Measurement of gravity at sea and in the air. *Rev. Geophys.*, **5**, 477–526.

LaCoste, L.J.B., Ford, J., Bowles, R. & Archer, K. (1982) Gravity measurements in an airplane using state-of-the-art navigation and altimetry. *Geophysics*, **47**, 832–7.

Milsom, J. (1989) *Field Geophysics*. Open University Press, Milton Keynes.

Nettleton, L.L. (1971) *Elementary Gravity and Magnetics for Geologists and Seismologists*. Monograph Series No. 1. Society of Exploration Geophysicists, Tulsa.

Nettleton, L.L. (1976) *Gravity and Magnetics in Oil Exploration*. McGraw-Hill, New York.

Ramsey, A.S. (1964) *An Introduction to the Theory of Newtonian Attraction*. Cambridge University Press, Cambridge.

Torge, W. (1989) *Gravimetry*. Walter de Gruyter, Berlin.

Tsuboi, C. (1983) *Gravity*. Allen & Unwin, London.